COMPACT NEUTRON SOURCES FOR ZERO KNOWLEDGE WARHEAD VERIFICATION USING EPITHERMAL NEUTRON TRANSMISSION ANALYSIS

By

Ezra Max Engel

B.S., Physics, United States Military Academy, 2017

SUBMITTED TO THE
DEPARTMENT OF NUCLEAR SCIENCE AND ENGINEERING

IN PARTIAL FULFILLMENT OF THE REQUIREMENTS FOR THE DEGREE OF
MASTER OF SCIENCE IN NUCLEAR SCIENCE AND ENGINEERING

AT THE
MASSACHUSETTS INSTITUTE OF TECHNOLOGY
JUNE 2019

Signature of Author: _____
Ezra Max Engel
Department of Nuclear Science and Engineering
15 May 2019

Certified by: _____
Areg Danagoulian
Norman C. Rasmussen Assistant Professor of Nuclear Science and Engineering
Thesis Supervisor

Certified by: _____
Richard Lanza
Senior Researcher, Laboratory for Nuclear Security and Policy
Thesis Reader

Accepted by: _____
Ju Li
Battelle Energy Alliance Professor of Nuclear Science and Engineering
and Professor of Materials Science and Engineering
Chair, Department Committee on Graduate Students

Compact Neutron Sources for Zero Knowledge Warhead Verification via Epithermal Neutron Transmission Analysis

by

Ezra Max Engel

Submitted to the Department of Nuclear Science and Engineering
On 15 May, 2019 in Partial Fulfillment of the Requirements
For the Degree of Masters of Science in Nuclear Science and Engineering

ABSTRACT

In anarchic international environments, verification methods improve the viability of arms control agreements and disarmament measures by allowing party states to escape the security dilemma. However, warhead verification requires confident assurance of warhead authenticity while protecting design information about the interrogated object. Zero-knowledge physical cryptography provides a solution to the verification paradox by introducing system designs that do not require electronic information barriers and protect sensitive information during measurement. Compact epithermal neutron sources enable the verification process to occur on-site and minimize the security risk of transporting special nuclear material to dedicated verification facilities. Experimental results demonstrate the feasibility of a tomographic approach to zero-knowledge physical cryptography, and MC simulations offer promising results for compact epithermal neutron sources.

Thesis Supervisor: Areg Danagoulian
Title: Norman C. Rasmussen Assistant Professor of Nuclear Science and Engineering

Contents

1 Introduction

Over the past two decades, the North Korean and Iranian nuclear programs have renewed interest in arms control, disarmament, and counter-proliferation. This interest has lead both to new bilateral treaties between the U.S. and Russia such as the New Strategic Arms Reduction Treaty (START) and collaborative efforts to curb weapon development in non-nuclear states through sanctions and negotiations. These efforts culminated in the Joint Comprehensive Plan of Action which greatly restricted Iran's capability to weaponize its nascent nuclear program. Whether these same efforts will succeed in North Korea remains to be seen.

Over the past fifty years, arms control agreements have been highly successful at reducing the global nuclear weapon inventory (mostly through bilateral agreements between the U.S. and Russia). Figure 1 shows the estimated global nuclear warhead inventory over the past 70 years. Researchers in disarmament give special attention to the U.S. and Russia (then the Soviet Union) as these two countries have possessed over 90% of the global stockpile at every point in the nuclear age.

The growing concern over nuclear proliferation has generated renewed interest in warhead verification research. Historically, nuclear arms control verification has focused on delivery vehicles, since they constitute a good proxy for strike capability and are easy to verify by national technical means. No arms control agreement has ever attempted to verify the authenticity of the warheads themselves. This has created a large global surfeit of non-deployed nuclear warheads (in stockpiles, long-term storage, and/or awaiting dismantlement).

A warhead verification regime must simultaneously accomplish two seemingly contradictory objectives. (1) The host country must be completely confident that the inspecting country will not obtain any sensitive design information about her weapons. (2) The inspector must authenticate the host's weapons to verify compliance to the pertinent agreement. Historically, verification systems incorporated either a template-based or attribute-based approach combined with an electronic information barrier (IB) to protect the host's design information. In a template-based approach, measurements are to be compared against a "fingerprint" for a known warhead, often selected at random from a host country's ICBM or cruise missile arsenal. In an attribute-based approach, the verification body selects a universal set of criteria for weapon designs that are compared against the host's interrogated warheads. In both cases, the monitoring country takes direct measurements of the weapon, but the information is encrypted electronically before read-out. This electronic encryption process, the IB, remains one of the most contentious design element in these verification systems [1].

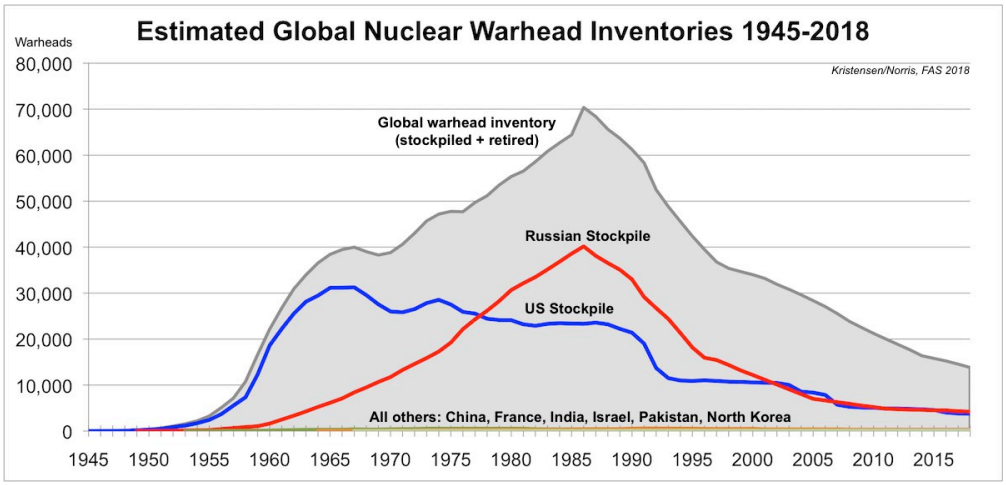

Figure 1: Estimated global nuclear warhead inventories over time. A large fraction of the overall decrease can be explained by a bilateral shift to more accurate weapons in the 1970s, and the collapse of the Soviet Union in the late 1980s. However, arms control agreements and their respective verification systems, in particular the Intermediate Nuclear Forces Treaty (1987), are also a major factor in the success of historical disarmament efforts. [2]

New approaches to verification have reduced reliance on IBs by offering viable alternatives. Instead, these systems—pioneered at Princeton University [3], and MIT [4]—use physical processes to encrypt sensitive design information before measurement. Physical cryptography simplifies the design of these systems and has the potential to increase international confidence in the viability of warhead verification for international arms control agreements.

In this thesis, we attempt to contextualize the importance of these new approaches and introduce novel techniques in physical cryptography and neutron time-of-flight (TOF) instrumentation. We begin with a justification of disarmament efforts generally, which some critiques have denounced as destabilizing [5] [6]. We then provide a brief history of previous arms control efforts and challenges. Finally, we introduce a new set of techniques that offer promising results for physically encrypted warhead verification.

This thesis contains nine sections. Section II examines the implications of normal accident theory for stochastic risk involving nuclear weapons. Section III explores the historical priorities of arms control and non-proliferation agreements. Section IV examines the generalized international problem of disarmament using the lens of game theory and international relations paradigms. Section V examines verification strategies for enforcement and arms control. Section VI gives an introduction to new research in physical cryptography and novel weapons verification techniques. Section VII examines results for an experimental validation of zero knowledge physical cryptography for warhead verification. Section VIII examines the design and use of compact epithermal sources for on-site verification. Section IX offers some

conclusions on the future landscape of verification technology and systems. Ultimately, we conclude that zero-knowledge technologies offer a valuable enforcement mechanism for future disarmament agreements by increasing both detection fidelity and confidence in information security, and that developments in compact sources and measurement techniques make a warhead disarmament effort increasingly feasible.

2 Complex Organizations and Normal Accidents

The U.S. Department of Defense and international equivalents have a long history of nuclear near misses. In the thirty-four years of the U.S. nuclear weapons program the DoD experienced *thirty-two* broken arrow incidents (nuclear accidents grave enough to endanger the American public) [7]. Any one of these incidents could have potentially resulted in a catastrophic loss of American life. While no similar concrete numbers exist for the Soviet nuclear program during the same time, it is likely that the USSR experience a comparable number of accidents. A growing body of literature in organizational psychology and systems engineering suggests that these types of accidents are guaranteed consequences of complex organizations.

2.1 The American Nuclear Establishment and Normal Accidents

Given the tremendous size and complexity of the U.S. government, the alarming frequency of nuclear accidents is unsurprising. Many organizational theorists promote a normal accident approach to complex systems and hazardous material. Normal accident theory was proposed in 1984 by Charles Perrow and requires that (1) the system is complex, (2) the system is tightly coupled, and (3) that the system has catastrophic potential. Normal accident theorists also frequently frame organizational failures as the result of friction between disparate interests within large organizations [8]. Subsequent developments in normal accident theory have also introduced the concept of human reliability into the framework. So, in addition to Perrow's initial requirements for systematic failure, we can add a fourth risk-multiplying factor: (4) human error [9].

1. Three primary organizations are responsible for overseeing nuclear safety and weapons management in the United States—the Air Force, the Navy, and the Department of Energy. These organizations have their own command structures with limited communication between them. They each contain multiple layers of commands, research groups, and authority structures. The U.S. nuclear apparatus is highly complex.

2. Nuclear weapons maintenance, storage, and security are generally handled by either the Navy or Air Force (although the national labs conduct frequent diagnostics as well).

The DOD uses a highly centralized system of checklists and maintenance priorities to manage its weapons systems, and this approach is rigidly standardized across the arsenal. The U.S. nuclear apparatus is tightly coupled [10, 11].

3. The U.S. stockpile consists of weapons with yields in the hundreds of kilotons. While these modern warheads are much smaller than the megaton warheads of the cold-war, an accident involving any one of them could still easily cause thousands of deaths. In the same vein, theft of nuclear weapons material (or a fully intact weapon) would constitute a massive national security threat. The U.S. nuclear apparatus has catastrophic potential.

4. The U.S. stockpile is staffed and maintained by 18, 19, and 20-year-old airmen and sailors. These junior enlisted personnel are frequently commanded by officers with a similar dearth of experience. During the 1980s, propellant transfer systems teams would routinely fill maintenance buckets with hydrazine and shoot at them with oxidizer-filled ping pong balls to entertain themselves during 14 hour shifts. While liquid-fuel rockets have been phased out of the stockpile, inexperienced young men still play pivotal roles in the maintenance and deployment of our nuclear weapons. The U.S. nuclear apparatus is vulnerable to human error [11][12].

The interactive complexity of these American organizations is mirrored in other national nuclear weapon programs. According to normal accident theory, this level of complexity guarantees failure pathways that are virtually unpredictable. These unforeseeable pathways can lead to catastrophe. The 1980 Damascus Titan missile explosion constituted one of the worst nuclear accidents in U.S. history. Describing the event, one of the airmen summarized the incredulity of the failure.

> One dropped socket that A, should have let's just say not dropped; but B, should have never got past a platform; C, shouldn't have hit the thrust mount; D, shouldn't have hit the missile. If it hit, it shouldn't have punctured a hole in it. I mean there are so many things that shouldn't have happened, but one dropped socket wiped out an entire nuclear missile system. One dropped socket, nine-pound socket, took it all out. There's no one that thought that scenario out. [11]

These types of system accidents are nearly impossible to forecast, and thus nearly impossible to prevent. The risk of failure inevitably grows with the size and complexity of the system, so in a super-large, hyper-complex system like the U.S. national security apparatus catastrophic failures are not just possible, but inevitable [12].

2.2 Institutional Risks

Normal accident theory has implications beyond the prediction of Broken Arrow incidents. The same dynamics that motivate disasters like the Damascus missile explosion can also confound attempts to make rational, informed decisions about the deployment of these weapons in conflict. During the height of the Cold War, the possibility of a Soviet decapitation strike directed at senior civilian and military leadership posed a grave command and control threat. This possibility was troublesome in the U.S. but considerably worse in Western Europe, which lacked an early warning system to detect an incoming Soviet attack on NATO command bunkers. The potential chaos resulting from a decapitation attack sensitized military leaders to the potential first-strike scenario, and kept them on a hair-trigger alert. It also meant that strategists only had minutes to plan a response upon the detection of an incoming attack. Over-sensitivity in both the U.S. and Soviet early warning systems further increased the likelihood of a false alarm—and subsequent response [12, 13].

The development of a national nuclear program can also substantially alter the political landscape in which decisions are made, further complicating a nation's organizational structure and increasing the risk of a nuclear strike. An underappreciated impact of national nuclear infrastructure are the substantial political and bureaucratic influences that the nuclear establishment can have on national decision making. The caché afforded to nuclear establishments in many countries affords them significant power to expand beyond their original mandates. This influence was apparent in the development of both India's and Pakistan's nuclear weapon programs, and remains a concern for potential nuclear proliferators such as Iran [14].

Even without the influence of nuclear establishments, nuclear weapons substantially increase the consequences of organizational miscalculations. This was most obvious in tense, high-stakes standoffs such as the Berlin Airlift (1948) and the Cuban Missile Crisis (1962). Nuclear weapons and first strike scenarios also posed serious challenges to conventional command and control structures within the armed forces—increasing the risk of a false-alarm, accidental nuclear conflict. Normal accident theory suggests that these scenarios are enabled by the same factors which facilitate broken arrow incidents: complex, tightly-coupled organizations with catastrophic potential. In tense international standoffs, these risks were further exacerbated by the potential for human error.

3 Nuclear Arms Control and Disarmament

Over the past 60 years, nuclear powers and the international community seem to have grown increasingly intolerant of nuclear risk. Despite consistent improvements in international safeguards and the end of the Cold War, the world has continued pursuing nuclear arms control, negotiating over a dozen agreements since 1970. The growing willingness of global powers to restrict delivery vehicles and nuclear testing reflects a rising global awareness and disapproval of the deployment and possession of nuclear weapons. This political and popular opposition is not a recent development. These movements have been around for almost as long as the nuclear weapons themselves.

3.1 Historical Disarmament Movements

The efforts of the Manhattan Project reached a climax on July 16th, 1945 with the Trinity nuclear test at Alamogordo, New Mexico. When the Gadget device detonated with a yield of 20 kT, Robert J. Oppenheimer, the project director, is alleged to have quoted the Bhagavad Gita, "I am become death, destroyer of worlds." Less than 1 month later, on August 6th, the United States dropped Little Boy on Hiroshima. Three days later, the U.S. dropped Fat Man—a weaponized iteration of Gadget—on Nagasaki. The bombs killed over 120,000 people, and on August 15th, Imperial Japan surrendered to Allied forces on the USS Missouri [15].

The bombings of Hiroshima and Nagasaki were indisputable demonstrations of the destructive potential of nuclear technology. Survivors of the explosion recount the indiscriminate carnage and unanimously express support for international disarmament efforts [16][17]. These horrors loomed over the global geopolitical landscape as nuclear technology proliferated to the Soviet Union, the United Kingdom, France, and China over the next two decades.

These technologies spread in spite of growing popular protest against the use and development of nuclear weapons. In Japan, these movements were spearheaded by the hibakusha (people affected by the bombings) who effectively used Hiroshima and Nagasaki as international symbols of protest and opposition. In the United States and U.K., disarmament movements gained traction in the 50s among pacifists, scientists, and world federalists. The latter two groups were particularly sensitive to the security dilemma (see Section IV) and strongly advocated for the creation of a strong world government as a solution. The French public, deeply concerned about the prospect of yet another global war, reportedly harbored a "repugnance for the use of these weapons except in the direst circumstances" [6]. In the Soviet Union, party leaders led efforts to stigmatize nuclear weapons in order to delegitimize U.S. military advantages in Europe. While these movements were originally agitated by scientists, pacifists, and world government enthusiasts, the ideas and motifs slowly percolated

into broader society throughout the fifties and sixties [6].

3.2 Previous Treaty Designs

Growing public opposition eventually culminated in the signings of the Partial Test Ban Treaty in 1963 and the Treaty on the Non-Proliferation of Nuclear Weapons in 1968. The NPT ushered in an age of multilateral arms control agreements that included the SALT I (1972) and SALT II (1979) talks, the INF Treaty (1988), START (1991), the Comprehensive Test Ban Treaty (arbitrated in 1996 but never ratified), and New START (2010) [6][18]. Most theorists and strategists agree that these arms control agreements have strengthened the international order and decreased the likelihood of nuclear mishaps [19].

Arms control agreements and test-ban treaties also played a crucial role in military de-escalation and confidence building during the Cold War. The Partial Test Ban Treaty (1963) was the first major multilateral effort at nuclear arms control. Negotiated between President Kennedy and Secretary Khrushchev, the agreement effectively ended atmospheric testing. Outside of Chinese and French resistance, the PTBT was received with almost universal adulation [6].

The mounting popular will to curb the testing and potential use of nuclear weapons also facilitated the Treaty on the Non-Proliferation of Nuclear Weapons in 1968. By this time, France and China had both developed their own versions of the A-bomb, and were enthusiastic signatories. Worries over potential nuclear catastrophe and populist sentiment compelled all but three countries to sign the agreement. The nonsignatories—India, Pakistan, and Israel—would all develop their own nuclear weapon programs over the next few decades in response to particularly acute security dilemmas [20].

The seventies and eighties saw a procession of bilateral agreements between the United States and the USSR targeted at weapon delivery vehicles. SALT I (1972) resulted in the Anti-Ballistic Missile Treaty which restricted the development and deployment of anti-ballistic missile systems. SALT II (1979) substantially curtailed development of new missile systems and also restricted the number of deployed MIRVs (multiple independently targeted reentry vehicles) for both countries. The INF (1988) eliminated all intermediate-range nuclear delivery systems deployed by the U.S. or USSR [21].

These agreements targeted delivery vehicles in lieu of actual warheads. Both countries were able to use their national technical means to verify the dismantlement of the delivery vehicles. Verification of the warheads constituted a significantly more difficult technical problem that policy makers declined to address [22]. These international agreements were instrumental in decreasing the number of deployed nuclear warheads by changing the incentives of countries

facing a security dilemma. Despite initial skepticism these agreements ultimately proved to be highly effective international motivators for disarmament efforts.

4 Obstacles to Disarmament

The disarmament problem can best be understood in the context of the three major schools of thought in international relations: realism, liberalism, and constructivism. In realist approaches such as balance of threat, nation-states execute policies as rational actors in an anarchic international order [23]. States respond rationally to threats by increasing defenses, and they use their militaries to gain strategic advantages if they believe that the benefit of doing so outweighs the cost. Liberalism promotes international cooperation and organizations as a means by which individual states can solve the security dilemma and avoid an arms race. Constructivism emphasizes the importance of cultural factors and ideology in steering the decision-making of states. Together, the three schools outline a set of obstacles to disarmament but also suggest a set of solutions.

This section uses game theory to examine the implications of realism, liberalism, and constructivism for arms control and disarmament. For a note on interpreting game tables, see Fudenberg [24].

4.1 Realism

The realist school of thought has a history that extends as far back as Thucydides, who used realist theories in his History of the Peloponnesian War in 431 BC [25]. The school boasts an impressive stable of thinkers and writers that includes Niccoló Machiavelli (1532), Thomas Hobbes (1651) [26], and Carl von Clausewitz (1832) [27]. It has influenced statesmen and diplomats like Otto von Bismarck, Henry Kissinger, and George Kennan.

At its core, realism has four primary axioms.

1. The international system is anarchic.
2. The actors in this anarchic system are states.
3. States are rational actors.
4. States are concerned primarily with survival [23].

In response to anarchy, states build defenses in order to bolster their own security. This build-up, in turn, forces other states to build their defenses. This cycle of escalation is defined

		State 2	
		Arm	Disarm
State 1	Arm	(-20, -20)	(+10, -30)
	Disarm	(-30, +10)	(0, 0)

Table 1: A game table depicting payoffs from a two state game in which both actors have the option to arm or disarm. Though both actors would prefer to remain in a disarmed state, the dominant strategy for both states is to arm.

as the *security dilemma* and has manifested itself in arms races throughout history, perhaps most vividly during the Cold War.

The security dilemma is an international extension of the prisoner's dilemma, introduced by mathematician, John Nash, in 1951 [28]. In the international version of the prisoner's dilemma, we have two states, each with an option to arm or disarm. In this game, players derive utility from increasing their relative position of strength, so the benefit of mutual armament or disarmament is zero. However, because building and maintaining a large military is expensive (whereas not having a military is free), mutual armament is a suboptimal outcome for both states. Large standing armies also increase the risk of the nuclear accidents and accidental false-alarm conflicts outlined in Sections I and II. For the sake of building a concrete game table, we can define the payoff from an increase in relative strength as (+30,-30) and the cost of arming as (-20). The resultant game table is shown in Table 1.

In the the security dilemma, because states cannot be confident about the covert actions of the opposing player, they are forced to arm themselves to avoid being cheated. In this way, even though both states would prefer to mutually disarm, they are forced to arm anyway. In purely realist scenarios, the disarm/disarm box is an unstable equilibrium, and states will fail to cooperate.

4.2 Liberalism

Liberalism critiques realism by emphasizing the power of international organizations and NGOs to shape international collaboration. The theory also claims that variations in the structure of national governments have significant affects on the decision-making processes of states. (A frequently cited piece of evidence in support of this is the apparent unwillingness of democracies to fight wars with each other—conflicts disproportionately involve autocratic states). Liberal orders have the potential to significantly affect the payoff structure of the security dilemma by introducing international organizations and verification regimes. By creating systems of international enforcement and compliance, states can be significantly

		State 2	
		Arm	Disarm
State 1	Arm	(-40, -40)	(-10, -30)
	Disarm	(-30, -10)	(0, 0)

Table 2: When the punishment for defections is added, it substantially changes the incentive to cheat on disarmament agreements by increasing the cost of arming, and the disarm/disarm strategy becomes a stable equilibrium.

		State 2	
		Arm	Disarm
State 1	Arm	(-20, -20)	(-5, -35)
	Disarm	(-35, -5)	(0, 0)

Table 3: When the benefit to cheating is reduced, we stabilize the disarm/disarm equilibrium for the game. Both states are able to disarm without fear that the other will cheat.

more confident in the viability of arms control agreement. [29]

International enforcement and inspection regimes impact the payoff structure in two important ways. First, international organizations can impose sanctions, or other punishments, on states found to be in violation of disarmament agreements. These punishments are highly costly for the violating country, especially in a tightly coupled international economic system. These punishments can change the payoffs by substantially increasing the cost of arming (-20). The resultant game table is shown in Table 2.

Regular inspections also substantially decrease the potential gains from cheating. Inspection regimes limit the amount of undetected progress that a country can make towards affecting the balance of power. They provide early warning, and the other players can respond appropriately, sharply decreasing the expected value of arming. We can represent this in the game table by shrinking the payoff from cheating to (+15,-15). This result is show in Table 3.

Combining these two effects can result in a substantial increase to the expected viability of an arms control agreement. Liberal international orders generally represent effective solutions to the collective action problem but they require verification to work effectively.

4.3 Constructivism

Constructivism recognizes the importance of popular will and ideological symbols in shaping national decision making. There are many examples in the literature of ideology playing large roles in national decision making in the United States [6], Germany [30], the Soviet Union [31], and the Middle East [32]. These ideological forces have the potential to significantly

		State 2	
		Arm	Disarm
State 1	Arm	(-20, -20)	(+10, -50)
	Disarm	(-50, +10)	(+20, +20)

Table 4: A populist pacifist movement has the potential to overcome the security dilemma by increasing the benefits of disarmament. In this case, the equilibrium is stabilized by significantly increasing the benefit of disarming.

impact the incentives to arm or disarm in the security dilemma.

Ideologies of nationalism and militarism can substantially increase the cost of disarming, especially if national nuclear programs become symbols of modernity and technological progress as happened in Pakistan and India [14]. Likewise, populist pacifist and disarmament movements could substantially increase the benefit to disarming. These effects drive incentives and decision making in opposite directions. The effect of a pacifist movement (+20 for disarmament) is shown if Table 4.

Combinations of ideological strategies and strong international organizations are both potential means to escape the security dilemma. Though populist movements can be powerful, they are also, by nature, uncontrollable. In systems design, we should focus on the development of strong international enforcement regimes to ensure agreement viability. However, in order for these regimes to effectively discharge their responsibilities, they need verification technologies and systems to monitor compliance.

5 Warhead Verification and Enforcement

5.1 Roles of Verification in Arms Control

Warhead verification is an important aspect of arms control and has an essential role in future disarmament strategies. It facilitates viable agreements and treaties in two primary ways. (1) Verification systems provide a deterrent against cheating on the agreement by increasing the probability of discovery and subsequent punishment. Through consistent and frequent inspections, they also decrease the potential benefits of violations by restricting timelines for undetected illicit development (e.g. US-Soviet verification organizations, and facility inspections in Iran). (2) Verification systems represent an important confidence building measure for treaty viability. Consistent and impartial verification regimes increase transparency and confirm that all parties are adhering to the agreement conditions. We have already seen the impact that international verification regimes have on treaty viability

through the historical success of arms control agreements. By promoting trust and punishing violators, verification regimes increase the viability and longevity of these agreements [33] [34].

Tolerance-level for undetected violations is an essential element of verification design. As many authors have noted, a verification regime that guarantees a 100% detection rate would be highly invasive, and potential signatories would almost certainly reject it [33]. As such, practical verification regimes need to be appropriate for an agreement's objectives. A verification regime may miss small violations, but as long as these violations do not substantially alter the balance of military power, the regime remains valid. In many cases, strong verification regimes may, nonetheless, be necessary for treaty viability. Strong regimes are particularly important in situations that involve technically capable and aggressive states, lack of a unified international security effort, or possible technical breakthroughs and political breakdowns [22].

5.2 Historical Verification Regimes

Verification has been an integral element in previous arms control designs. Most agreements over the past sixty years have established independent verification institutions to inspect for agreement compliance. These institutions have generally been bilateral (mostly between the U.S. and USSR), but are often regional or even global.

The United States and the Soviet Union have included stipulations for independent verification institutions in almost every one of their treaties between 1960 and the present day. The Threshold Test Ban Treaty (1974) created the Bilateral Consultative Commission to inspect and monitor further nuclear tests. SALT II (1979) created a standing consultative commission to enforce compliance for arms reduction. The Intermediate-Range Nuclear Forces Treaty (1987), START I (1991), and START II (1993) all provided for independent verification organizations—called the Special Verification Committee, the Joint Compliance and Inspection Committee, and the Bilateral Implementation Coalition, respectively [33, 6].

Regional verification bodies have also played an important role in arms control. These include EURATOM and the Agency for Control of Armaments for Western Europe, OPANAL in Latin America, the Argentine-Brazilian Agency for Accounting and Control of Nuclear Materials, the Joint Nuclear Control Commission for Korea, and the African Commission on Nuclear Energy. Since the 1960s, the IAEA has served as the primary global verification body [33, 6].

None of these regimes have successfully targeted actual warheads. We have enjoyed relative success in monitoring fissile material and restricting delivery vehicles, but warheads have escaped the scrutiny of verification institutions for over 50 years. Until present, arms

control agreements have ignored the nuclear components of weapons because verification is intensely difficult. The nuclear components are generally quite small, usually on the order of a few kilograms of fissile material, and are thus more difficult to verify without exposing sensitive design information [22]. Delivery vehicles can be counted using national technical means such as spy satellites, but the warheads themselves generally require more direct interrogation. The unique challenges inherent to warhead verification have led to a range of technological and systems-based approaches.

5.3 Verification Approaches and Technologies

The sensitivity of warhead design information exacerbates the verification paradox. The monitoring country must be confident that the warhead is authentic, but the host country must be certain that the monitoring country does not acquire any classified design information [35]. To solve this problem, most traditional designs conceal direct warhead measurements behind electronic information barriers (IBs).

Verification systems must also satisfy a number of other requirements. These criteria are more fully explored in the literature [36], but generally include:

- preventing unauthorized operation and use,
- protecting classified data,
- preventing unauthorized and undetected modification of the system, especially in ways that allow a party to extract classified data,
- not producing false negatives
- being transparent (to facilitate inspection),
- including diagnostics that verify correct operation without disclosing classified data,
- and detecting errors during operation.

In short, the system needs to perform all the functions of a standard radiographic measurement without disclosing any classified data to the inspectors operating it.

There are two major approaches to verification design: template based and attribute based. A template-based approach compares signals from interrogated warheads against the known "fingerprint" of an authenticated weapon. The template is selected to guarantee its authenticity—potentially at random from a launch-ready ICBM. Template based approaches are effective for efficiently verifying large numbers of identical weapons configurations [1].

The attribute based approach uses a mutually agreed upon set of attributes to test interrogated weapons against. These systems are more susceptible to clever cheating strategies, but they have two advantages. First, they can be used to verify nearly any potential warhead, universalizing a single mode of operation. Second, they do not require storage of sensitive weapon design information in the "fingerprint" like template based designs. Potential attributes in these systems include: presence of plutonium or uranium-235, isotopics, mass of fissile material, symmetry, and the presence of high explosives [1]. These criteria describe a large majority of deployed warheads, but may be vulnerable to clever hoaxing scenarios that use asymmetric pits, exotic fissile material (potentially neptunium), or innovative radiation shielding. Due to these vulnerabilities, template-based approaches are generally considered to be more secure [1].

The measurements used to verify the warhead can use either passive or active interrogation. Passive interrogation utilizes detectable signals intrinsic to the fissile material. These can include gamma ray emissions from radioactive decay, as well as neutron and gamma ray detection from spontaneous fissions in plutonium and uranium. While gamma rays are more readily detectable, they are also significantly attenuated by the weapons material, especially if the tamper is constructed from tungsten instead of depleted uranium [37, 38]. Because passive interrogation methods can be implemented using only a single detector, they are highly agile and have been used successfully to detect and characterize attributes of Soviet warheads on SLCMs [39].

Brookhaven and Sandia National Labs have developed high fidelity, template based, passive systems for use in warhead verification. In 1988, Brookhaven introduced CIVET—a Controlled Intrusiveness Verification Technology—as a potential verification system. CIVET uses passive gamma and x-ray radiography with systems of detectors to measure elements of pit geometry [40] and was successfully used to verify weapons in field trials in the late 1990s [41]. Sandia developed TRIS—Trusted Radiation Identification System—in 2000. TRIS utilizes a high purity germanium detector to measure gamma emissions from plutonium using a model of the scattering continuum in the intravenous materials [42]. Both systems utilized a series of computational information barriers with dedicated trusted processors to maintain information security [40, 42].

Oak Ridge National Labs uses active instead of passive interrogation in their verification designs. The NMIS—Nuclear Materials Identification System—uses a californium-252 neutron source to interrogate potential fissile material. The system uses plastic scintillators and pulse shape discrimination to detect gammas and neutrons from induced fissions [43]. NMIS did not contain specifications for a devoted information security system, instead suggesting that information security could be achieved through the use of IBs developed by Brookhaven

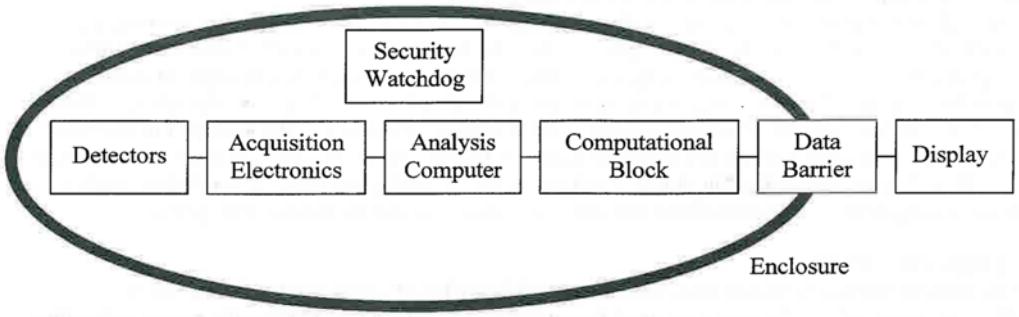

Figure 2: A model for information barrier design. Direct measurements, acquisition, electronics (multi-channel analyzers), and data analysis are performed before a final data barrier. The inspector receives a Boolean output (TRUE for weapon, FALSE for counterfeit). [44]

and Sandia. In general, active interrogation systems allow the monitoring party to verify the authenticity of warheads with higher fidelity, but require an external radiation source which introduces additional logistic and technological burdens. Others have proposed gamma radiography for active interrogation, but the rapid attenuation of photons in high-Z materials have generally made neutrons the preferred option [38].

5.4 Information Barriers

The national lab proposals (with the exception of NMIS) use computational information barriers to protect the host country's design information. Traditional information barriers (IBs) use system, hardware, and software design to prevent the disclosure of classified measurement information while providing diagnostic confidence to the monitoring country. A basic layout for information barriers is shown in Figure 2.

Computational information barriers are designed to promote transparency for the host and monitor. They employ dedicated CPUs with highly restricted functionality to analyze the data and encrypt it before display. They attempt to minimize electromagnetic emanations. They utilize simple detectors and multi-channel analyzers to acquire the measurement information. Despite these attempts to maximize transparency, inspection of these systems can remain difficult and opaque. Host countries generally insist on supplying the integrated system to minimize the potential for information leakage, but this invites opportunities of subterfuge and hoaxing [45].

Some of these systems become so complex that their own design can become classified, further obfuscating the ostensible transparency of the information barrier [35]. Additionally, for template-based designs, storage of highly sensitive "fingerprint" information remains

an unsolved problem for IB designers. The host fears that the monitor will use it to obtain the design information while the monitor fears that the host will tamper with it, so custody becomes a major point of contention. The inherent complexity and opaqueness of computational IBs undermines the political feasibility of their implementation.

6 Zero-Knowledge Physical Cryptography

To solve many of the problems posed by IBs, researchers at Princeton and MIT have proposed an entirely new approach to verification. These new methods use the template-design with active interrogation, but use physical processes combined with zero-knowledge proof protocols to ensure that no direct measurement of the object is ever taken. This physical cryptography obviates the need for information barriers, simplifying design and improving transparency.

These new verification approaches rely on zero-knowledge (ZK) protocols developed by Goldwasser in 1988. Zero-knowledge protocols verify a claim without informing the verifier about why the claim is valid. [46]

An effective example is posed on Wikipedia using marbles. A regime needs to verify that the number of marbles (x) in two cups is identical without knowledge of the number of marbles in either cup. To accomplish this, the host prepares two buckets with 100-x marbles in each bucket. The verifier then chooses which cup to empty into which bucket. If either bucket does not contain 100 marbles, the verifier knows that the host was lying. As this measurement is repeated, the verifier gains confidence that the number of marbles in each cup is identical without ever learning the value of x. The confidence associated with a verification process using N number of trials can be described by $P(N) = 1 - 0.5^N$.

It is important to note that the marble example and many recent developments in verification are not, strictly, zero-knowledge. In the marble example, for instance, the verifier learns that there are fewer than 100 marbles in the original cups. While there are ways to perform the marble example that satisfy a strict zero-knowledge protocol, in practice, verification approaches do not need to meet strict ZK standards in order to be useful. Because we can be fairly certain that every warhead contains weapons-grade uranium or plutonium, a system that potentially reveals the presence of a fissile isotope in a warhead does not violate reasonable standards of information security.

The Princeton group successfully implemented this approach for a zero-knowledge system with fast-neutron radiography. In their system, two arrays of identical preloaded detectors are configured by the host country. These detectors are preloaded with the negative of the radiograph from the warhead template. The monitoring country then selects which array will measure the template and which array will measure the submitted item. If the host country

has attempted to defraud the inspectors by changing the preloads in one of their arrays there is a high probability of being caught when the monitor performs multiple measurements [3].

This system improves on IB designs because by eliminating the reliance on electronic encryption and simplifying overall system design. However, it faces two major disadvantages.

First, the system is isotopically insensitive, and may be vulnerable to hoaxing scenarios. Because it relies primarily on fast neutron interactions, there are multiple combinations of isotopes that can result in similar overall neutron cross sections and thus similar overall measurements. Specifically, the system may be insensitive to substitutions of weapons grade plutonium for reactor grade plutonium in potential hoaxes. Research to solve this problem through additional measurements (particularly of spontaneous fissions in Pu-240) is ongoing [47].

Second, the detector preload restricts potential detector technology to superheated emulsion detectors and neutron activation detectors. Superheated emulsion detectors only operate at about 1% efficiency, and are highly temperature sensitive which results in long measurement times and a necessity for precise temperature controls. Neutron activation detectors (often Zirconium or Indium based) operate at an even lower efficiency (0.25%). Additionally, the preloads for both detectors decay over time, so the preload and measurement must be precisely timed to ensure information security. [3]

To solve many of these problems, researchers at MIT have combined isotopically sensitive approaches with new zero-knowledge protocol design. These new systems use epithermal neutron radiography in lieu of the fast neutron radiography used by Princeton and NMIS. Neutron resonance transmission analysis (NRTA) is highly sensitive to isotopic variations in interrogated materials due to isotopically unique resonance absorption spectrums. These cross sections are nearly impossible to hoax and can be used to precisely determine isotopic abundances in interrogated material. Using time-of-flight techniques, the energy spectrum for incident neutrons on a detector can be reconstructed with high precision (around 1 eV), and analyzed for verification purposes. Absorption resonance regions for plutonium isotopes are shown in Figure 3 [48].

Early iterations of NRTA did not implement a zero knowledge protocol to protect the classified measurement information. New research at the MIT Laboratory for Nuclear Security and Policy has incorporated these zero-knowledge design protocols into new system designs.

These designs call for the measurement of an aligned pit and reciprocal object to physically encrypt both isotopic and geometric design information about the interrogated warhead. The reciprocal is a physical object designed by the host country with the same isotopic characteristics as the warhead. When appropriately aligned with an interrogated pit, the areal density across the pit-reciprocal object is uniform, shown in Figure 4. Functionally the

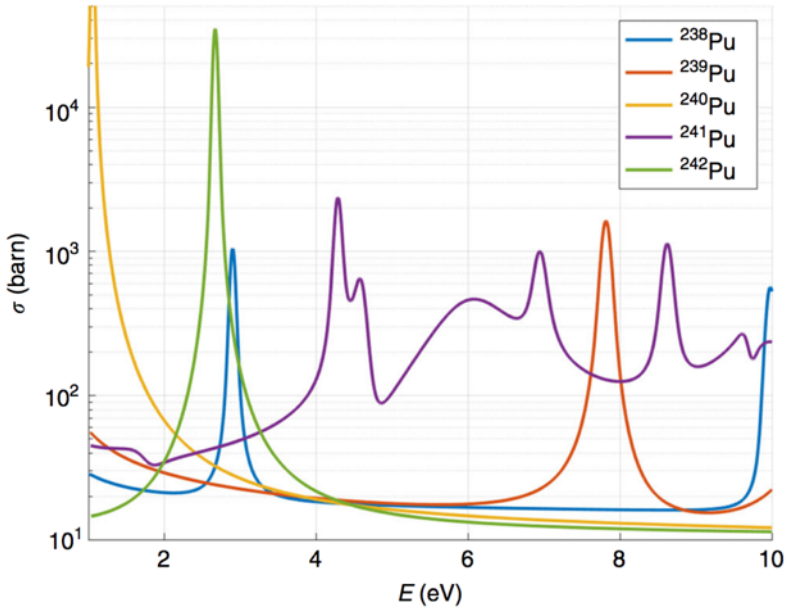

Figure 3: Neutron absorption resonances are plotted for a variety of plutonium isotopes. The unique shapes of these spectra allow precise reconstructions of isotopic abundances in interrogated material. [48]

reciprocal preloads neutron attenuation across each linear path through the material. Monte Carlo simulations have shown that the reciprocal can be designed such that measurements through the pit-reciprocal object reveal no useful geometric information about the warhead [48].

Isotopic information can also be physically encrypted by adding homogeneous material to the reciprocal of an unknown isotopic constitution. Ultimately, the measurements will only determine the isotopic abundance across line integrals through the pit-reciprocal object. If appropriately designed, it is impossible for inspectors to reconstruct the isotopic characteristics of the isolated pit object [48].

The reciprocal-based epithermal design offers two distinct advantages over the Princeton proposal. First, due to its isotopic sensitivity, it is sensitive to a broader range of possible hoaxing scenarios. Second, because it does not rely on preloaded detectors, detector selection is less constrained by the design criteria. This aspect of the design could substantially simplify the verification system by eliminating the need for precise timing of preload decays and also eliminate the issues of detector temperature sensitivity. The MIT design could also improve the counting accuracy of the system by utilizing modern solid-state detectors with efficiencies approaching 80% [49].

The reciprocal based approach also faces two primary challenges. First, precise alignment

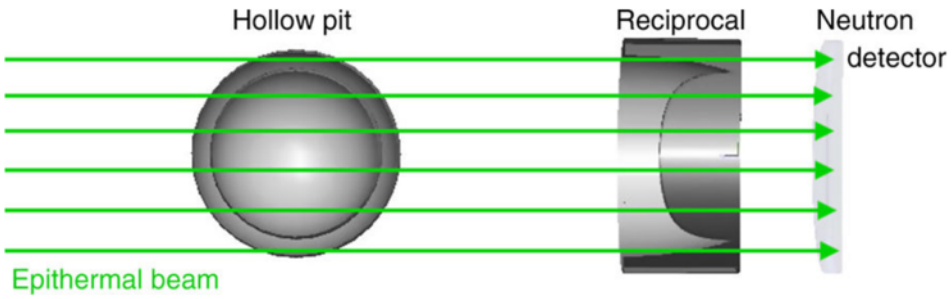

Figure 4: The pit-reciprocal object is designed to ensure that areal isotopic densities are constant across the object. This ensures a constant rate of neutron attenuation, and provides geometric information security for the host. Simulations have shown that neutron in-scattering does not appreciably impact this geometric security. [48]

of detector and reciprocal objects is essential for geometric and isotopic information security. Small deviations in alignment could result in significant information leakage. One potential solution to this alignment sensitivity is to decrease the resolution of the detector array. Another possible solution utilizes single-pixel comparative tomography [50] which is further discussed in Section 7. Second, collimated beams of epithermal neutrons are somewhat more difficult to produce than collimated beams of fast or thermal neutrons. Recent work has demonstrated the feasibility of thermalized neutron spallation as a viable source for epithermal neutrons for neutron powder diffraction [51]. Moderated Cf-252 sources are another potential epithermal source for NRTA. LinAc and DT neutron sources are also viable for verification applications. Due to the diversity of options and techniques, access to adequate neutron sources should not pose a serious obstacle for verification, especially in countries with robust nuclear infrastructure.

This epithermal approach also requires that the warhead be fully dismantled before the verification process. Otherwise, the hydrogenous high-explosive surrounding the pit will significantly attenuate the epithermal beam. Verification approaches employing passive gamma spectroscopy and fast neutron detection do not require prior disassembly. For different applications, such a requirement might present a major obstacle for implementation; however, because verification is focused on the support of disarmament efforts, verified pits would have been marked for disassembly anyway. The requirement that warheads be disassembled prior to measurement becomes significantly more modest and feasible with the understanding that the warheads would have needed to have been disassembled eventually regardless of the physical limitations of the measurement. For an more in-depth discussion of the non-technical verification procedures, see Kemp [4] and Hecla [48].

7 Zero-Knowledge NRTA Tomography

While the verification system proposed by Hecla et al. provided promising results for the feasibility of zero-knowledge system and physical cryptography, it introduces new security and technical challenges to the verification process. [48]

While the geometric reciprocal mask does ensure geometric and isotopic information security when properly aligned with the interrogated pit, small misalignments between the two objects could result in a substantial leak of both geometric and isotopic information. Depending on the resolution of the neutron detector, alignment errors as small as 50 micrometers could reveal the radius, thickness, and enrichment of an interrogated warhead. This concern was emphasized during multiple conversations with specialists at the National Labs. These vulnerabilities could be mitigated through precise alignment, coarser imagers, and the introduction of films to “smear" the image. However, the alignment issue remains an important failure point for the system, and concerns about information security cannot be easily dismissed when the system involves the use of images.

Another difficulty in the reciprocal mask approach is the construction of a complex reciprocal—and possibly multiple reciprocals depending on machining tolerances—for each warhead design in a host’s stockpile. The manufacture of these reciprocals would require relatively large amounts of enriched fissile material and precise machining in each design case. Additionally, the large amount of fissile material involved in the construction of these masks would require designers to consider criticality as a potential failure point. Though the reciprocal might be sliced into sections to mitigate these criticality concerns, such a demand would further complicate the alignment issues discussed previously, and amplify concerns about information security.

Finally, the work completed by Hecla et al., relies only on Monte Carlo simulations for a proof of concept. Though MC simulations have proven to be a highly useful tool for feasibility studies and design optimization, an experimental verification of such a design would be essential before widespread adoption. These concerns combined with the need for an experimental validation of a physical cryptography system lead us to explore single-pixel tomography as a potential solution to both the security and technical concerns with previous work.

7.1 Configuration and Process

To avoid the use of a geometrically complex reciprocal mask and mitigate possible alignment issues, single-pixel tomography was considered as an alternative. Not only does tomography resolve the alignment concerns discussed previously, it also requires a far simpler experimental

set up. Such a design would require only a collimated neutron source, a test object, a simple encrypting filter, and a lithium glass neutron detector.

Geometrical uniqueness is determined by performing a series of random rotations between on axis measurements of a pit object. It can be shown that geometrical uniqueness only requires 3 to 4 measurements for single pixel tomography [4]. While it is possible to manufacture geometrically dissimilar objects that produce similar spectra, as the number of rotations increases, these hoax geometries rapidly become impractically complex. For each measurement the detector would measure the total flux of all neutrons transmitted through the source and provide geometrically and isotopically sensitive data that, when combined across different rotations, uniquely identify the fingerprints for genuine warheads.

To maintain information security with the single pixel system, an encrypting foil is placed into the beam line. The encrypting foil can be a simple plate with an isotopic composition similar to that of the pit object. With the inclusion of the foil, the detector measures only the combined attenuation spectrum of the pit plus the encrypting foil. With such a system, it becomes impossible to isolate and determine the enrichment of the pit as distinct from the encrypting foil.

The high-level approach to template-based warhead verification is discussed Hecla et al [48]. The inspecting country announces an inspection of a host country. A short time later, some random deployed warhead is removed from an ICBM or SLBM. If the inspector is concerned about hoaxing, it might remove multiple deployed warheads. The deployed warheads are measured to establish a unique fingerprint of authenticity. Measurements of candidate warheads are then compared to this authentic fingerprint to establish genuineness. Using the tomographic process described above, each measurement would consist of 5 steps.

1. The genuine reference warhead, the encrypting foil, and the neutron detector are aligned along the axis of an epithermal neutron beam. A full schematic for the measurement is show in Figure 5. The encrypting filter is manufactured by the host, and its precise geometric and isotopic composition is unknown to the inspectors; however, a treaty might enumerate a list of isotopes that such a filter was allowed to consist of. The encrypting filter would be composed of the same isotopes as the test object, and could be constrained to achieve some minimum flux at the detector surface. The host takes a spectroscopic measurements of the genuine warhead and observes the data. If the host approves the data, the inspectors may record the measurement for use as a fingerprint. If the host rejects the data, it is deleted and the measurement retaken.

2. The encrypting filter is left in place while the genuine reference warhead is replaced with a candidate warhead. A measurements is taken under the conditions described in

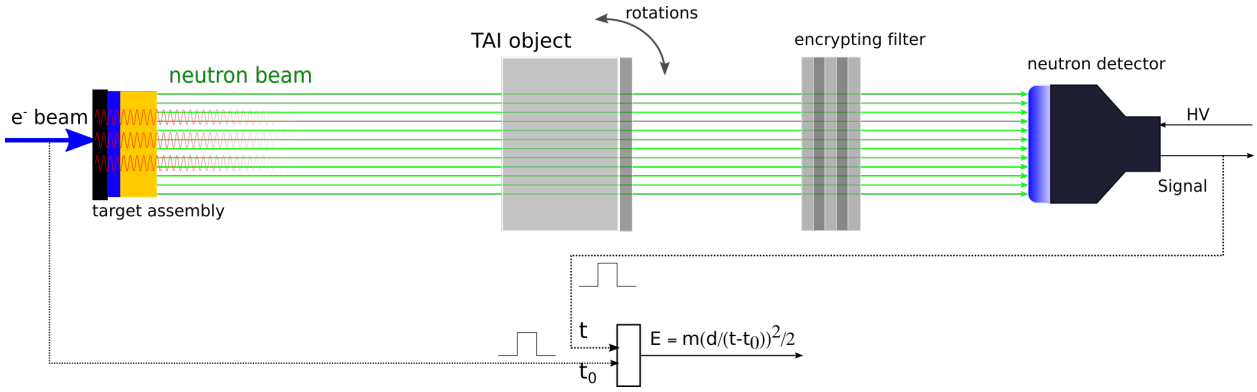

Figure 5: A schematic for the tomographic pit measurement. Measurements are taken of the pit and encrypting foil which provides isotopic and geometric information security. Geometrical uniqueness is achieved via rotations.

step 1. This step can then be repeated for as many candidate warheads as desired.

3. The spectrum from the genuine reference warhead is compared with the spectrum of each candidate warhead. If a statistical χ^2 test produces a test statistic above a certain threshold (as determined by treaty partners) the interrogated object is declared a hoax, and appropriate punitive action as determined by the treaty is initiated against the host. If the result of the χ^2 test does not exceed the established threshold, the measurement proceeds to step 4.

4. The genuine reference warhead is now placed back into the beam line, now with some specified random rotation. The rotation is generated by the inspector using a random number generator. At this time, the hosts replace the encrypting foil with a new filter to prevent differential analysis. The encrypting foil should always be replaced in between rotational measurements to maintain information security. Steps 1 to 3 are repeated for the new rotation and encrypting foil. The genuine warhead is measured and then replaced with a rotated candidate. The spectra are compared and if the χ^2 test exceeds an established threshold, the candidate is labeled a hoax.

5. Step 4 can be repeated any number of times to increase the geometrical sensitivity of the verification system. Based on previous work performed by [4], three rotations should be sufficient for a viable verification system, but this would ultimately be determined by treaty partners during negotiations.

Experimental work focused on determining the feasibility of this design for use in a verification regime. Measurements were performed at the Rensselaer Polytechnic Institute Gaerttner LINAC center, a facility optimized for neutron TOF cross section measurements.

The experimental set-up is discussed in-detail in the methods section. Ultimately the system was able to clear all genuine warhead candidates, and identify both geometric and isotopic hoaxes demonstrating a proof of concept for the zero-knowledge tomographic design. These results are discussed in-detail in the results section.

7.2 Methods

The Gaerttner LINAC center uses a 60 MeV electron beam to generate pulsed, moderated neutrons for TOF cross section measurements, and was constructed to support the U.S. Navy's reactor research in the 1960s. To generate neutrons, electrons are accelerated along the LINAC into a tantalum target where they create bremsstrahlung radiation as they slow down in the target. The bremsstrahlung radiation then impinges on the same tantalum target, where the high energy photons cause (γ,n) reactions in ^{181}Ta. ^{181}Ta is a weakly confined nucleus which can disintegrate above a threshold of approximately 8 MeV. The cross section for this reaction is shown in Figure 6.

The neutrons from photodisintegration are emitted isotropically from the tantalum target. They are then collimated and moderated into a low energy pulsed beam. After moderation, the neutron energies ranged from thermal to MeV, but a cadmium filter after the HDPE moderator eliminated the thermal flux before the start of the beam line. A small fission chamber within the beam line provided data to normalize for the small fluctuations in the beam flux. The beam path was kept at vacuum for all measurements, and used a lithium glass neutron detector for data acquisition with a beam path of 15.12 meters. The beam was collimated to a 4.7625 cm diameter before transmitting through the target and encrypting foil.

The target was contained within an aluminum box machined at MIT's central machine shop. The box was designed to rotate through a variety of angles without the need to unmount the sample from the beam line. The encrypting plates were mounted directly to sample holder in the beam line. The plates were manually swapped between different rotations. Figure 7 shows a schematic of the holder for the measurements. Due to relatively low interaction cross sections, the 1 mm of aluminum within the beam line did not significantly affect measurements.

7.2.1 Targets

Due to the lack of availability of plutonium and uranium for experiments, the targets consisted of proxies that were available in an academic setting. Such proxies needed to have epithermal resonance structures in the energy range between 1 eV and 200 eV. We used

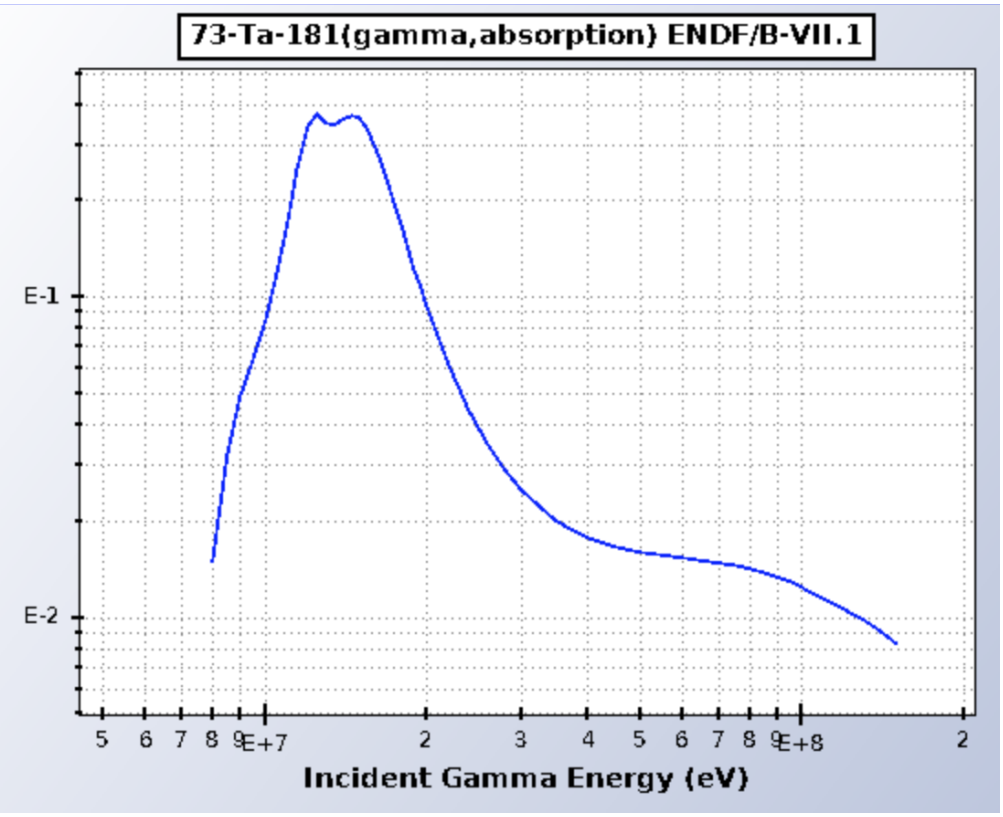

Figure 6: Cross section for photodisintegration of ^{181}Ta. Photodisintegration likelihood increases with increasing photon energy with a threshold at approximately 8 MeV. Photodisintegration allows even relatively low energy bremsstrahlung radiation to produce large numbers of neutrons. Cross section from ENDF data.

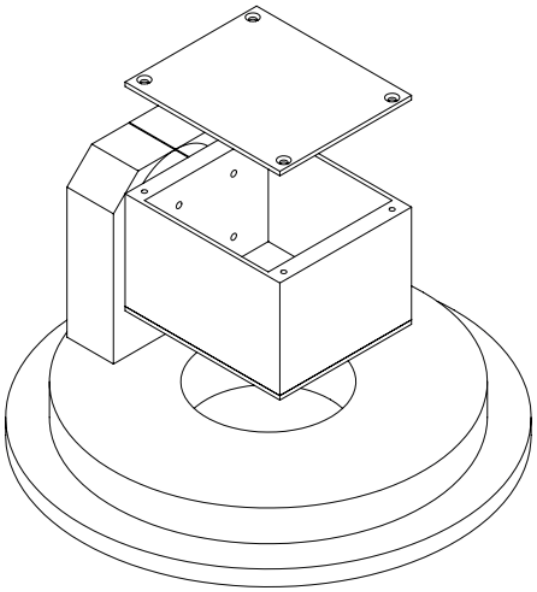

Figure 7: Schematic of the object holder. The interrogated object is contained within an aluminum box and suspended in the beam line. The box is able to freely rotate through any rotations of interest. The encrypting foil is mounted directly to the mounting plate during measurements.

natural molybdenum and tungsten for this purpose. In this experiment molybdenum was used as a proxy for ^{239}Pu (and ^{235}U) while tungsten was used as a proxy for ^{240}Pu (and ^{238}U).

We used simple cylindrical and box geometries instead of hollow pits—which are more typical in actual weapon designs—to simplify the manufacturing process. In our measurements, cylindrical configurations were a proxy for genuine warheads while a box configuration represented a geometric hoaxing attempt. All objects had a depth of 30 mm with a diameter (or side length for the hoax) of 50.8 mm.

The experiment took measurements of five proxy pit objects designed to evaluate possible failure points for the system. The geometric hoax was deliberately designed to be cleared by the first, on-axis measurement. This necessitated the use of rotations to identify the hoaxing attempt.

1. A genuine reference object consisted of 50.8 mm diameter cylinder with 27 mm of molybdenum and 3 mm of tungsten. This corresponded to a 90% pit enrichment.

2. A genuine candidate with identical geometry to the template. This was used to determine whether the system was able to clear honest objects.

3. An isotopic hoax at 50% enrichment with the same diameter as the template but with 15 mm of molybdenum and tungsten each.

Measurement	Enrichment	Shape	Rotation	Filter
Rotation 1				
Template	90	Cylinder	0°	9W6M
Genuine	90	Cylinder	0°	9W6M
Iso 50 Hoax	50	Cylinder	0°	9W6M
Iso 10 Hoax	10	Cylinder	0°	9W6M
Geo Hoax	90	Box	0°	3W2M
Rotation 2				
Template	90	Cylinder	45°	6W9M
Genuine	90	Cylinder	45°	6W9M
Geo Hoax	90	Box	90°	6W9M
Rotation 3				
Template	90	Cylinder	90°	3W12M
Genuine	90	Cylinder	90°	3W12M
Geo Hoax	90	Box	90°	3W12M

Table 5: List of experimental measurements. Measurements were chosen to identify potential failure points for the assembly. These included clearing genuine candidates, discriminating against isotopic hoaxes, and employing rotations to identify geometric hoaxes.Filter notation XWYM refers to X mm of tungsten and Y mm of molybdenum.

4. An isotopic hoax at 10% enrichment using 3 mm of molybdenum and 15 mm of tungsten.

5. A geometric hoax consisting of a 50.8x50.8x30 mm box at 90% enrichment (27 mm of molybdenum with 3 mm of tungsten).

The template was compared to the genuine pit and the isotopic hoaxes via a single on-axis measurement. It was compared to the geometric hoax using three different rotations at 0°, 45°, and 90°. The geometric hoax was only differentiated at the 45° and 90° rotations.

7.2.2 Measurements

The experiment consisted of 11 primary measurements taken over approximately 3 hours at the Gaerttner LINAC. A full list of primary measurements is shown in Table 5. Various encrypting foils were constructed from combinations of tungsten and molybdenum plates (each one 3mm thick). Filter notation XW6M refers to X mm of tungsten and Y mm of molybdenum.

The fission chamber was used to normalize any beam fluctuations that occurred over the 3 hour measurement time—such fluctuations proved to be minimal. The background was also measured and determined to be low relative to the flux of the beam line. Additional

measurements using a smaller collimator were not ultimately included in the analysis of the results.

7.2.3 Detector

The experiment used a simple lithium glass detector for neutron detection. Lithium glass detectors detect neutrons via $^6\mathrm{Li}(n,t)\alpha$ reaction. When a neutron interacts with ^{6}Li, the lithium breaks into an alpha particle and triton. Both of these charged particles scintillate in the glass which in turn is amplified by a photo-multiplier tube, and ultimately registered as an event by the detector.

Because the energy of the resulting alpha and triton are only loosely connected to the energy of the incident neutron, the original energy of the neutron is lost to the detector. The energy of neutrons cannot be easily measured directly as with other forms of radiation. The energy spectrum of transmitted neutrons needs to be reconstructed using other methods.

7.2.4 Time of Flight Reconstruction

The incident neutron energy spectrum was reconstructed using time of flight analysis. To improve the empirical accuracy of the reconstruction, an energy spectrum for 3 mm of tungsten was compared to cross section data from ENDF. The expected locations of the tungsten resonances were compared with the locations of those resonances in the data, and significant discrepancies began to appear at energies above 50 eV.

Using a two parameter fit for the flight path and t_0 somewhat improved the reconstruction, but nonlinearities in the time-to-energy transformation continued to introduce discrepancies into the reconstructed spectrum. Further analysis demonstrated that these nonlinearities were a result of variations in neutron moderation times. On average, lower energy neutrons exited the moderator more slowly than higher energy neutrons, since they had to spend additional time within the moderator to reach those lower energies.

Ultimately, we determined a relationship between neutron energy and moderation time (and thus t_0) using a specialized Monte Carlo simulation. The relationship between mean moderation time and detected neutron energy was well defined by a power law,

$$T_{mod}(E) = 2040 \cdot e^{-0.500 \cdot E} + 42.1 \quad ns. \tag{1}$$

When this power law was implemented to adjust the t_0 of incident neutrons, the TOF reconstruction became highly accurate, correctly predicting resonances at over 100 eV.

Ultimately, the accuracy of the TOF reconstructions had a minimal impact on direct chi-squared comparisons between various spectra. However, the accuracy of the reconstructions provided confidence that the measurements were physically accurate.

7.3 Results

Pure molybdenum and tungsten plates were measured to assess calibration and TOF reconstruction accuracy during analysis. The shapes of the molybdenum and tungsten spectra were referenced against the expected resonance locations and intensities for natural tungsten and molybdenum. The Joint Evaluated Fission and Fusion Nuclear Data Library (JEFF 3.2) was used for cross section data. After TOF modifications described in Section 7.2.4, the spectral and cross section data were in strong agreement with each other.

The comparisons between the genuine warhead and isotopic hoaxes are shown in Figure 8. The differences in the measured spectra are highly apparent even upon visual inspection, and the reduced chi-squared values for the each comparison reflect this high degree of separation. Because the resonant attenuation is highly nonlinear, it remains possible to differentiate the isotopic hoaxes even when the spectra are normalized for total integrated counts. This indicates that this method is sensitive to both total counts *and* spectral shape and is robust to a broader range of possible hoaxing scenarios that might employ HDPE to decrease absolute neutron flux homogeneously across the epithermal energy range.

A measurement along the z-axis for a specific geometry is sensitive only to the projection of that geometry (and its isotopics) on the axis of measurement. The transmission T for a an energy bin E and a spherically symmetric geometry can be approximated as

$$\ln T \simeq -\sum_i \frac{\sigma_i(E) N_{Av} \rho_i}{A_i} 2\pi \int_{\cos 1}^{\cos \theta'} \int_0^X f_i(r, \cos\theta) dr d\cos\theta, \tag{2}$$

where $\sigma_i(E)$, ρ_i, X, θ' and A_i are the cross section, density, total thickness, solid angle, and atomic number for isotope layer i of the object, respectively. $f_i(r, \cos\theta)$ is the fractional abundance of isotope i at a particular radial coordinate, and N_{Av} is Avogadro's number. The summation is performed across every isotope within the object, and the radial and polar integration occur over the range of the object's dimensions. The neutron detector effectively reduces this spacial integral to a single spectral measurement, and geometrical information is lost during this compression. However, further geometrical sensitivity can be gained back by performing multiple measurements at different rotations. Previous work has shown that if these rotations are random, only one or two of these rotations is necessary to guarantee the

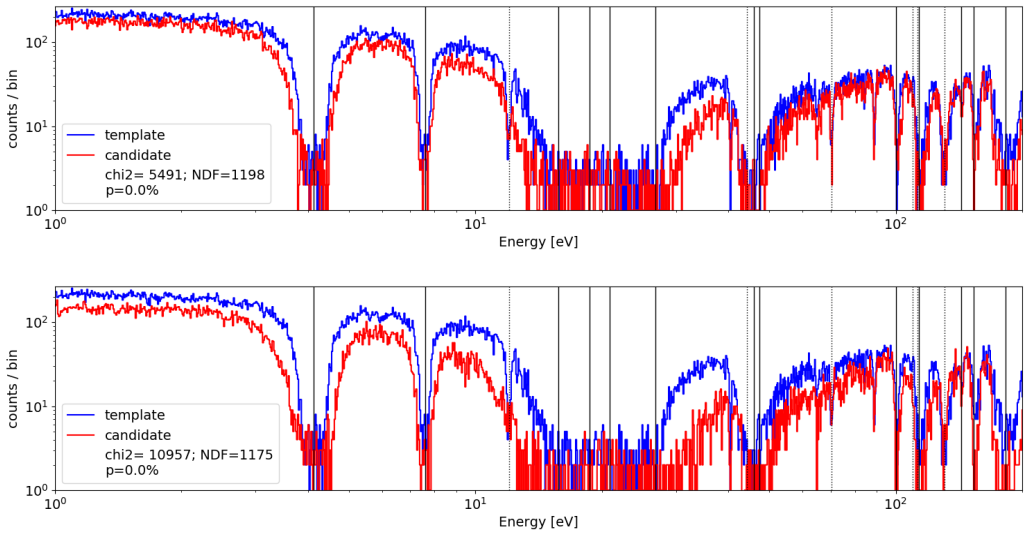

Figure 8: Histograms of neutron count energies, as reconstructed via the TOF technique, for two isotopic hoaxes. **a** The template data from an authentic reference of 90/10 Mo/W composition (blue) is compared to the data from a 50/50 Mo/W isotopic hoax (red). **b** The data from the authentic reference is compared to that from a 10/90 Mo/W isotopic hoax (red). The legend lists the χ^2 value, the number of degrees of freedom, and the corresponding probability (p-value) for the χ^2 test. Both hoaxes are rejected. The solid and dashed vertical lines denote the locations of some of the known tungsten and molybdenum resonances, respectively. Data collection lasted approximately five minutes per object.

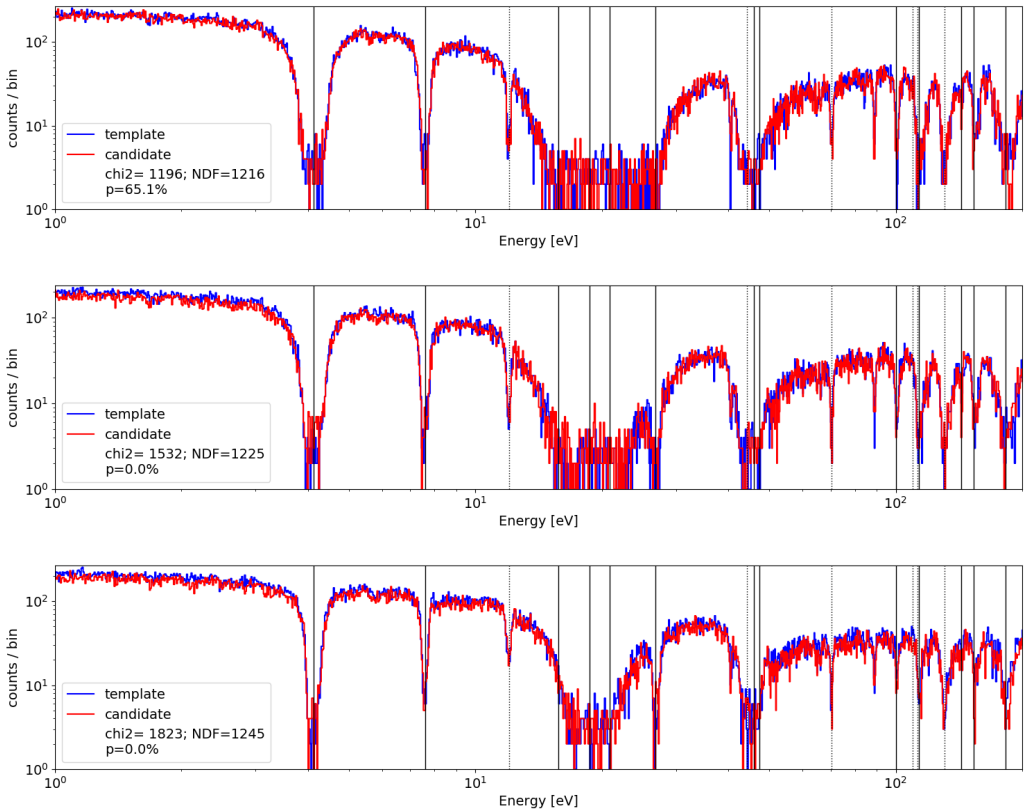

Figure 9: Histograms of neutron count energies, as reconstructed via the TOF technique, for a geometric hoax. The geometric hoax has been constructed as to have the same areal density along z-axis as the genuine reference. The template data from an genuine reference (blue) is compared to the data from the geometric hoax (red) at $\theta = 0°$ (top), $\theta = 45°$ (middle), and $\theta = 90°$ (bottom). As expected per design the $\theta = 0°$ yields a perfect agreement, as shown by the p-value. The rotations readily expose the hoax.

geometrical uniqueness of a given object.

In order to prevent differential analysis on the multiple measurements, it is essential that the host country have the opporunity to change the encrypting foil between rotational measurements. By swapping encrypting foil, the host country ensures that the degrees of freedom for the measurements exceeds the estimated parameters, and information security is preserved.

Figure 9 shows the comparison between the template and geometric hoax across three rotations of 0, 45, and 90 degrees. Due to a deliberate choice of hoax pit geometry, the geometric hoax initially clears the inspection when measured on axis at 0 degrees. However, additional rotations reveal the hoaxing attempt. Reduced chi-squared values for the geometric rotations are lower than those for the isotopic hoaxes but remain significantly large to confidently differentiate the geometric hoaxes with a p-value less than 10^{-5}.

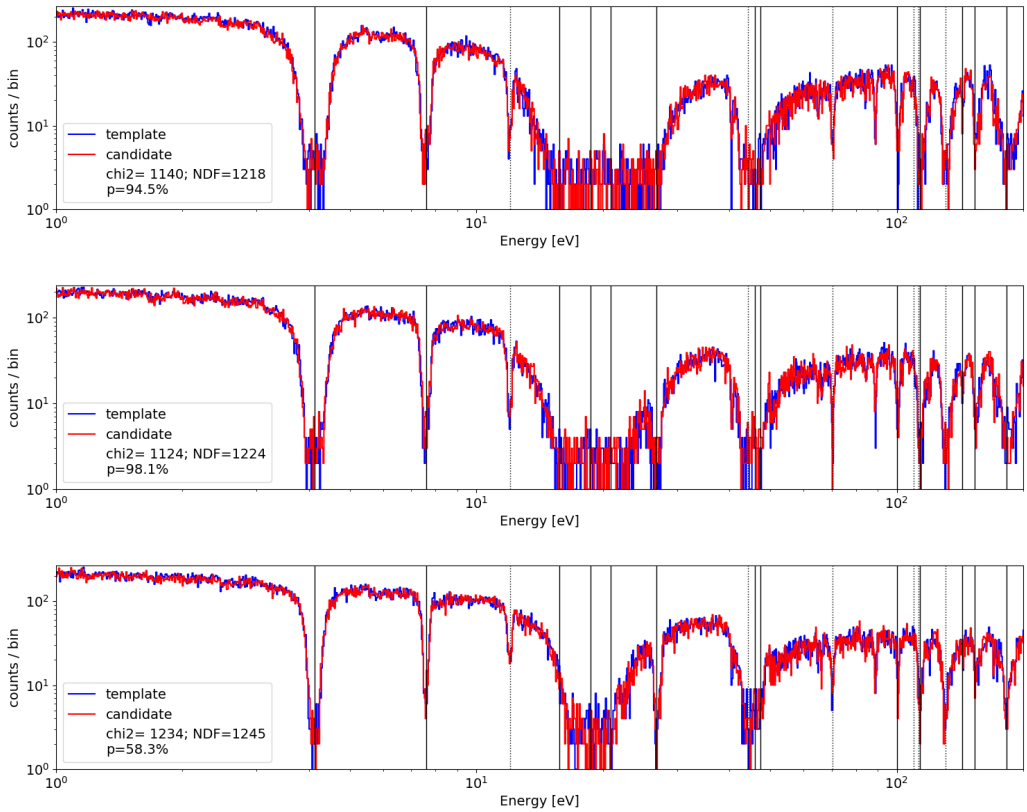

Figure 10: Histograms of neutron count energies, as reconstructed via the TOF technique, for a comparison between an genuine reference (golden copy, shown in blue) and an genuine candidate (shown in red). The measurements were performed at rotation angles $\theta = 0°$ (top), $\theta = 45°$ (middle), and $\theta = 90°$ (bottom). All comparisons yield p-values of 50-95%, indicating an agreement, and thus clearing the candidates as genuine objects.

To demonstrate that the system is able to clear honest objects, the spectra of the template were compared to that of an genuine candidate and statistically compared. Across all three rotations, the spectra of the two (identical objects) were consistent with each other. In a practical application of this system the host and inspector would both need to carefully monitor the beam stability and pit alignment in order to mitigate any false-positive measurements on genuine pits.

7.4 Discussion

Table 6 shows a summary of template, hoax, and genuine pit comparisons. The experimental results demonstrated a qualitative agreement with previous simulated work using JEFF cross sections. All isotopic hoaxes were effectively distinguished with a single measurement, and the tomographic approach allowed us to distinguish even a geometrically similar object with

Object	Rotation	χ^2/NDF	p-value	Decision
Isotopic Hoaxes				
Iso 50 Hoax	0°	5491/1198	0.00	Reject
Iso 10 Hoax	0°	10957/1175	0.00	Reject
Geometric Hoax				
Geo Hoax	0°	1196/1216	0.42	Accept
Geo Hoax	45°	1532/1225	0.00	Reject
Geo Hoax	90°	1823/1245	0.00	Reject
Genuine Candidate				
Genuine	0°	1140/1218	0.94	Accept
Genuine	45°	1124/1224	0.98	Accept
Genuine	90°	1234/1245	0.58	Accept

Table 6: Experimental Results. Comparisons of different spectra led to a rejection of hoaxes and a clearing of genuine candidates. The system was highly sensitive to isotopic hoaxing attempts. Though geometric hoaxes resulted in lower reduced chi-squared values, they were still large enough to achieve confident differentiation between the template and geometric hoaxes.

multiple rotations. Finally, the system was shown to be able to clear genuine objects with high confidence. All measurements were implemented with the use of encrypting plates to preserve information security, and sufficient statistics were gathered within 5 minute measuring times for confident candidate identification.

Despite the successes of this simplified approach to warhead verification and information security, after measurement and analysis, we determined two potential issues for practical application.

First, in certain cases, the measured object may not be a hollow sphere. This becomes problematic if the pit consists of a solid mass of plutonium or uranium. In these cases, the line integrals through the fissile material increase from 1-3 cm to 6-10 cm. In these cases, attenuation through the center of the object can reduce the statistical significance of measurements in that area. In these cases, inspectors must rely on attenuation through a relatively small band of neutrons at the edge of the object where the line integral becomes more tractable. While this does not render verification impossible, it does make it statistically more difficult.

While this technical dilemma might seem to undercut the reliability of this approach, politically, it is rather insignificant. The only nations that might employ these types of problematic design approaches are nations with nascent (and insurgent) nuclear weapons programs. These states are unlikely to be the main focus of future disarmament efforts which remain dominated by bilateral agreements between the U.S. and Russia. Additionally, should

these countries eventually become the targets of disarmament efforts, it remains unlikely that the U.S. will take the approach of arms control agreements. Past U.S. approaches have generally relied on coercive sanctions in support of these types of policy objectives. Finally, should a country's stockpile consist primarily of rudimentary fissioning sphere weapons, it is improbable that information security will be as important. Bare fissioning solid-spheres are less technologically unique, vulnerable, or sensitive as modern hollow-pit, boosted weapon designs.

Second, if the measured object is a hollow sphere, good forward models can lead to a loss of information security for the host country. Take, for example, a homogeneous, hollow-sphere, two-isotope pit described by three parameters: diameter, shell thickness, and enrichment. In the simple design proposed in this paper, the expected spectrum for a combined pit-foil measurement can be effectively described by five parameters. The attenuation spectra can be approximated as

$$\begin{aligned}\ln T[E] * \frac{A}{N_{Av}\rho} &= (N_p\sigma_1[E] + (1-N_p)\sigma_2[E]) \\ &\cdot \left(\int_{-\frac{d-t}{2}}^{\frac{d-t}{2}} 2 \cdot \left(\sqrt{\left(R+\frac{t}{2}\right)^2 - y^2} - \sqrt{\left(R-\frac{t}{2}\right)^2 - y^2} \right) dy \right. \\ &\left. + \int_{-\frac{d+t}{2}}^{\frac{d+t}{2}} 2 \cdot \sqrt{\left(R+\frac{t}{2}\right)^2 - y^2}\, dy \right) \\ &+ (N_f\sigma_1[E] + (1-N_f)\sigma_2[E]) \cdot x\end{aligned} \tag{3}$$

where N_p, N_f, d, t, and x are pit enrichment, foil enrichment, pit diameter, pit thickness, and foil thickness respectively. The cross sections for the two isotopes are known and can be referenced from a nuclear database to create a fully specified forward model of the expected spectrum. If the encrypting foil is simple plate, it may be possibly for the inspecting country to use a curve fitting algorithm to accurately fit the five parameter model using N bins of energy data (so long as N is greater than the number of parameters in the forward model).

This technique was tested analytically using cross section data from JEFF 3.2, and the SciPy curve-fit module was able to accurately reconstruct geometric and isotopic information from a given energy spectrum. In a practical application, this information problem can be mitigated by simply increasing the complexity of the encrypting foil. If the host country chooses a more complex (but still relatively simple) geometry other than a plane, it can effectively increase the degrees of freedom beyond the number of energy bins in the final measured spectrum. Additionally, due to high non-linearities in the attenuation effects, simple curve-fit algorithms become increasingly unstable in the presence of Poisson noise. This

greatly limits the precision with which a curve-fit algorithm could determine the parameters of the forward model even if the encrypting foil remains a simple plate.

7.4.1 Narrow Beam Construction

Significantly reducing the radius of the beam would also greatly reduce the efficacy of a parameterized forward model. If the beam is narrow relative to the scale of the measured object, differential analysis between the varying on-axis line integrals becomes virtually impossible. In the wide-beam case, the measured spectra is a linear summation of all the on-axis line integrals through the pit. The linear summation of exponential effects is what allows for reconstruction with good forward modeling. Using narrow beams, the spectra is reduced to the attenuation over a vary limited area of the pit. The inspector gains far less information per measurement which significantly improves information security. When combined with the encrypting filter, these types of measurements truly reveal no information about the warhead outside of the bounds that the inspector and host deem acceptable (maximal quantity of fissile material, minimum enrichment, etc.)

A narrow beam construction will also make the system significantly more sensitive to small variances in object geometry. The wide-beam is sensitive to macroscopic differences in the geometry of the measured objects, but remains insensitive to microscopic variations in the machining and surfaces of interrogated pits. Narrow beams would be significantly more sensitive to these smaller changes in geometry. In certain cases, the required geometric resolution might exceed the capabilities of NRTA tomography and would require the use of a dedicated imaging facility using a different approach to cryptography.

7.4.2 True Zero-Knowledge Modifications

The measurement of combined pit-foil objects is not a strictly zero knowledge scheme. Due to the nature of attenuative processes and additive line integrals through material, the tomographic design provides an estimate for the maximum amount of each measured isotope within the pit object. In a practical application of this design, it would benefit all treaty partners to specify minimum enrichment for all warheads. Using this method, an inspector might learn that the host's pits are *at least* 70% enriched with *at most* 10 kg of ^{239}Pu within the warhead. This does not represent any new, or useful knowledge gained by the inspector, because all modern warheads will generally conform to these two design principles. If a prospective treaty is intelligently written, it will allow for this manner of (useless) information leakage.

However, if both treaty partners insist that a verification regime must be strictly zero-

knowledge, the current design can be modified to adhere to that more rigid standard. making the spectra from attenuative processes truly zero knowledge generally requires spectral summation. Glaser et al. accomplish this by pre-loading bubble detectors with a geometrical inverse of a soon-to-be measured object [3]. Because the host is able to pre-load the detector array with an arbitrarily high (unknown) number of counts, the system is a truly zero knowledge system.

This same type of pre-load can be accomplished in the tomographic regime, except that the pre-load needs to occur concurrently with the measurement. Because the tomographic system uses lithium-glass electronic detectors, it excludes the possibility of a physical pre-load as described in Glaser et al. To facilitate a simultaneous pre-load, the tomographic system would likely need to include a secondary neutron beam incident on the detector. Such a beam could be run continuously, producing a steady beam of thermal neutrons. There is no known combination of physical isotopes that would create an inverted attenuation spectrum. However, because we rely on TOF to reconstruct the energy spectrum, such a system could use a combination of the thermal neutrons and a cadmium chopper wheel to perform a time-space transformations.

The wheel would be carefully designed and calibrated, such that the radial position of the wheel corresponded with a specific TOF reconstructed energy. The wheel could then be manufactured to produce the an inverted attenuation spectrum for a given isotopic/geometric pit configuration. If properly designed, such a system would eliminate the requirement of the encrypting foil entirely, and be a truly zero-knowledge system. Further work is needed to fully determine the practical feasibility of this type of implementation. Despite these advantages, the calibration of such a system would be incredibly sensitive, and greatly complicates the systems design. One of the primary advantages of such a tomographic system is its portability, simplicity, and ease of construction. Such a complication would undermine all of these design advantages and should only be pursued if the treaty partners are unable to agree on a minimum acceptable level of information leakage. In this instance, a policy solution is far preferable to the technological modification.

8 Compact Neutron Sources

The zero knowledge epithermal tomography approach described in Section 7 has shown to be a promising method for physically encrypted warhead verification. As described, the verification regime is isotopically and geometrically sensitive to various hoaxing attempts while protecting sensitive design information for host countries. Modifications described in Section 7.4.2 would render the system *truly* zero-knowledge though would significantly

complicate the overall design.

The primary disadvantage of epithermal NRTA is the current requirement of a large dedicated facility for neutron TOF measurements. Transporting candidate weapons to such a dedicated facility during a prospective disarmament process represents a significant security risk for both the host and inspector and may also complicate the verification of final weapon dismantlement if this occurs at yet another site. An ideal verification regime would verify the warheads AT the site of prospective disassembly. This would require the use of mobile compact neutron sources capable of TOF reconstruction. Such a system would not necessitate the precision of the Gaerttner facility or facilities for cross section measurement and might be feasibly accomplished with a system that fits within a standard cargo container for easy shipping and transportation.

This section explores ongoing work in the development and optimization of such an instrument. We have focused our efforts on disarmament applications, however there may be extensions to archaeology, paleontology, and a number of other fields that require on-site isotopically sensitive characterization of unknown materials.

8.1 Monte Carlo Simulations

Monte Carlo simulations were used to model various shielding and moderator configurations to optimize performance. Due to the relative expense of constructing a physical system, and the difficulty of the neutron diffusion problem for complex geometries, Monte Carlo simulations proved to be the most effective technique for optimizing the system design. The purpose of the simulations was to optimize two criteria: shielding configuration and moderator thickness. The optimization of the shielding geometry improved the TOF energy reconstruction and reduced the background. The optimization of the moderator improved the efficiency with which fast neutrons from the source were moderated to the desired epithermal range.

8.1.1 Simulations

Simulations for viable shielding geometries were performed with grasshopper, a GDML-based Geant4 application [52]. Two series of simulations were performed to optimize both the moderator thickness and shielding geometries for the compact source. All simulations used a 14.1 MeV isotropic neutron source to simulate neutrons produced by a compact DT source. Neutron generation was modeled as an instantaneous, zero-width pulse. At later stages in the optimization analysis the time distribution of the output was smeared with a square function of a width 5μs, which is the shortest possible pulse width of the Thermo Electron P325 neutron generator [53].

As a way of increasing computational efficiency, a dedicated and separate simulation was performed to determine the optimal moderator thickness. This simulation involved a parallel beam of neutrons traversing a cylindrical high-density polyethylene moderator of 10 cm diameter and a thickness which was varied between 1 and 20 cm. The neutrons were recorded by a tally plane at the rear surface of the moderating cylinder, with the neutron beam impinging along the z-axis of the moderator cylinder. All forward scattered neutrons were detected immediately upon exiting the moderator. This configuration allowed for both increased computational efficiency and the ability to perform a differential analysis of optimal moderator geometries for maximizing epithermalization efficiency. It also enabled analysis of moderation time distributions for various moderator thicknesses. Longer moderation times ultimately smear the energy reconstruction by introducing uncertainty into the actual TOF measurement. See Section 8.1.2 for more detail.

The shielding optimization was performed via a series of different simulations with realistic laboratory geometries, including: (1) the D-T source shielding, collimation, and moderation; (2) air, which scatters the neutrons; (3) a tungsten-silver target, as a test object; (4) the laboratory's concrete walls, which result in room return; and (5) an idealized detector with 100% detection efficiency, surrounded by its own shielding to reduce room return. Since the moderator thickness was determined in the prior epithermalization simulations (see Section 8.1.2), these new simulations only iterated over the shielding and collimation geometries. Moderator thicknesses were held constant at 10 cm for all geometries.

The need to suppress room return and collimator in-scattering constrained the choice of materials and geometries. Viable shielding geometries required 75 cm of 5% borated polyethylene surrounding the source to moderate and attenuate the off-axis neutron flux in order to reduce thermal and epithermal background from room return. To minimize the impact of in-scattering, the collimator walls and cylindrical detector shielding required a compound with a high molar ratio of boron. Boron carbide was determined to be the ideal material for these components. A schematic of the optimized shielding geometry is shown in Figure 11. The target was chosen to consist of a mix of tungsten and silver for two reasons. First, these elements have very clear resonances in the ∼eV range, and thus can be used for an optimization analysis applicable to most actinides (e.g. ^{235}U, ^{238}U, and most plutonium isotopes). Second, both tungsten and silver are easily available in the necessary quantities for performing follow-up experimental studies.

Finally, the shielding design required the use of three cadmium filters in the beam path. One filter at the collimator exit eliminated the thermal flux exiting the moderator via ^{113}Cd(n,γ)^{114}C reaction's "threshold" at 0.5 eV and reduced the thermal background in the room. Two other filters placed at either end of the cylindrical detector shield prevented

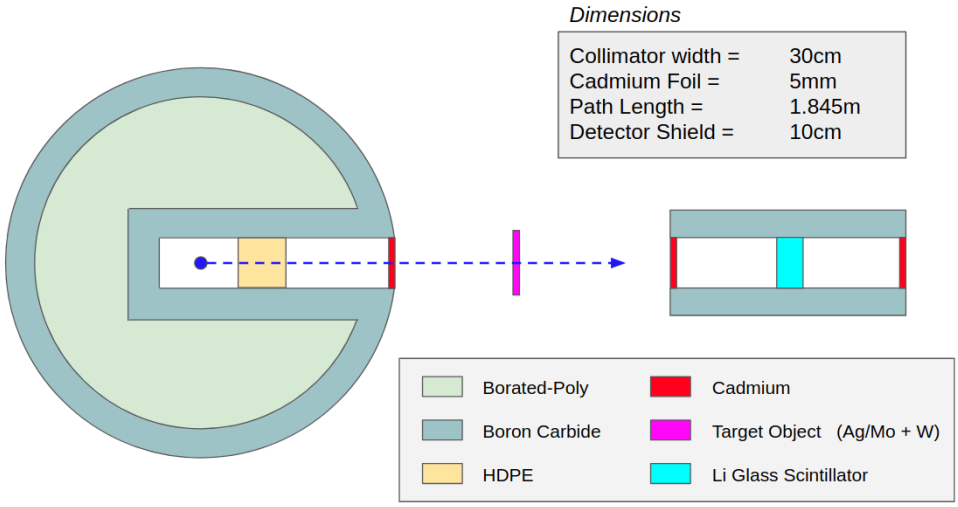

Figure 11: Schematic of a compact NRTA platform using a DT source (not to scale). The portable source required large amounts of shielding around the neutron generator to both reduce the intensity of room return and to decrease the dose rate. The design used boron-carbide scatter absorber for chemical and structural stability.

thermal neutrons from entering the detector shield. See Figure 11 and Table 7 for the full geometry of the system.

8.1.2 Moderator Optimization

The moderator thickness was optimized using two criteria: epithermal efficiency and precision in TOF reconstruction. The epithermalization efficiency was defined as the fraction of incident 14.1 MeV neutrons that were slowed down into the energy range 1-30 eV and exited the rear surface of the moderator. The process of moderation introduces uncertainty into the TOF reconstruction. An optimal moderator maximizes the epithermalization efficiency and introduces minimal error to the TOF.

Figure 12 shows a plot of overall epithermalization efficiency vs. moderator thickness. The ideal moderator thickness, from an efficiency perspective, proved to be approximately 10 cm with minimal change in performance between 7 and 11 cm. The initial increase in efficiency is primarily a result of additional scatters of 14.1 MeV neutrons as the moderator thickness increases. The decrease beyond 11 cm occurs because down-scattering from the epithermal to thermal ranges begins to dominate the initial epithermalization at large moderator thicknesses.

The efficiency of epithermalization, even when optimized at 10 cm was determined to be $(9.3 \pm 0.1) \times 10^{-5}$. Even at the optimized moderator thickness, the thermal flux at the rear surface of the moderator is two orders of magnitude higher than the epithermal flux since increasing cross sections at lower energies lead to a build-up of thermal neutrons in the

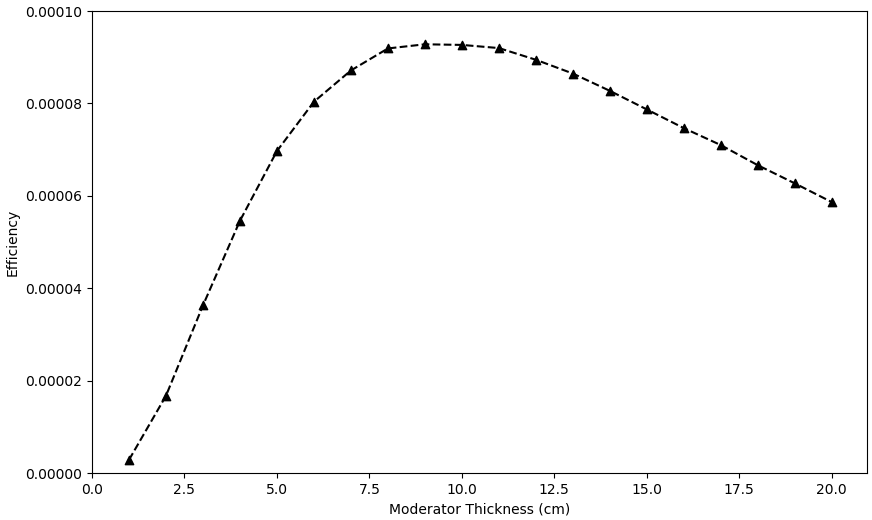

Figure 12: Epithermalization efficiency of various moderator thicknesses. The maximum efficiency occurs at approximately 9 cm with a stable range between 7 and 11 cm. Competing processes of epithermalization and thermalization create the maxima behavior.

system. The cadmium filter however removes most thermal events.

The simulated data was also analyzed to understand the effects of moderation on the widening of the input epithermal pulse and the subsequent smearing in the energy reconstruction. This analysis showed that the time distribution of the epithermalized neutrons was not significantly impacted by increases in moderator thickness beyond 3cm. The distribution for the error in energy due to the moderation, defined as the difference between the TOF reconstructed energy and the actual energy for each neutron is plotted in Figure 13 for various moderator thicknesses. It is apparent that moderator thickness has a negligible effect on the accuracy of TOF reconstruction in the epithermal regime.

The overall effect of thermalization time on the energy reconstruction accuracy can be further decreased by increasing the distance between the moderator and the detector apparatus. This is also true for other effects which lead to uncertainty in actual epithermal TOF and thus energy uncertainty. It can be shown that the uncertainty in TOF relates to uncertainty in energy via $\delta E/E = 2\delta t_0/(t-t_0)$, where E is energy, t is the TOF, and t_0 is the time-zero, and δt_0 is the uncertainty in time-zero [48, Suplemental Note 1]. Increasing the length of the flight path increases the energy resolution of the system due to $t-t_0 = d\sqrt{2E/m}$, where d is the flight path and m is neutron energy. This however also decreases the overall counting efficiency by $\sim 1/d^2$. Figure 14 shows the effect of increasing flight path on the TOF reconstruction deviation. A more detailed discussion of pulse width and flight path

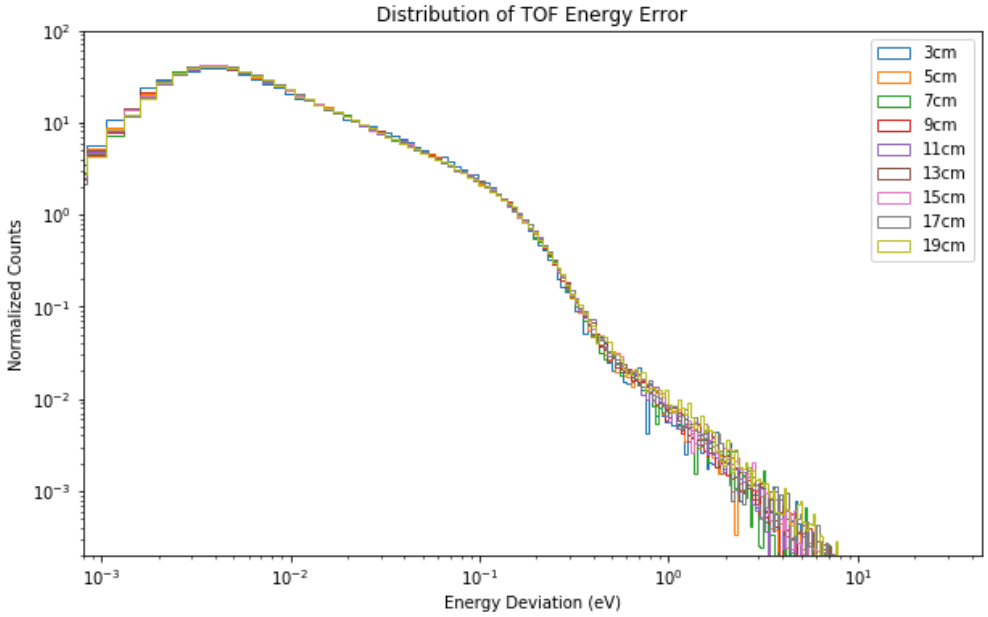

Figure 13: Distribution of neutron's TOF-reconstructed energy deviation, $\delta E = E - E_{tof}$ for a detector distance of 1.87 m, and a variety of moderator thicknesses marked in the legend. The distribution follows a power law with a power of -2 for lower deviations and approximately -0.5 for higher deviations.

distance optimization analysis is discussed in Section 8.3.

The negligible impact of the moderator thickness on TOF resolution is a result of both relatively short flight paths within the moderator itself and the physical nature of moderation. Because the relationship between moderator thickness and TOF reconstruction is negligible, the overall performance is optimized only by the epithermalization efficiency, which is maximized at approximately 10 cm. Most epithermalization occurs 3 cm from the rear surface of the moderator, so flight paths must be adjusted for thicker moderators.

8.1.3 System Geometry

The optimized shielding geometry is described schematically in Figure 11. This configuration succeeded in both minimizing the impacts of room return and in-scattering on the detected spectrum. Moderation and shielding of the DT-source required 1.5 tonnes of borated polyethylene encased in a boron-carbide shell. Designs that incorporated less HDPE or eliminated the shell suffered significant leakage from the outer surface of the absorber-moderator sphere, resulting in high intensities of room return and epithermal background. We thus omit these configurations from this discussion.

The collimator was also plated with boron carbide to minimize the probability that a neutron scattered off or through the surface of the collimator would be measured in the TOF

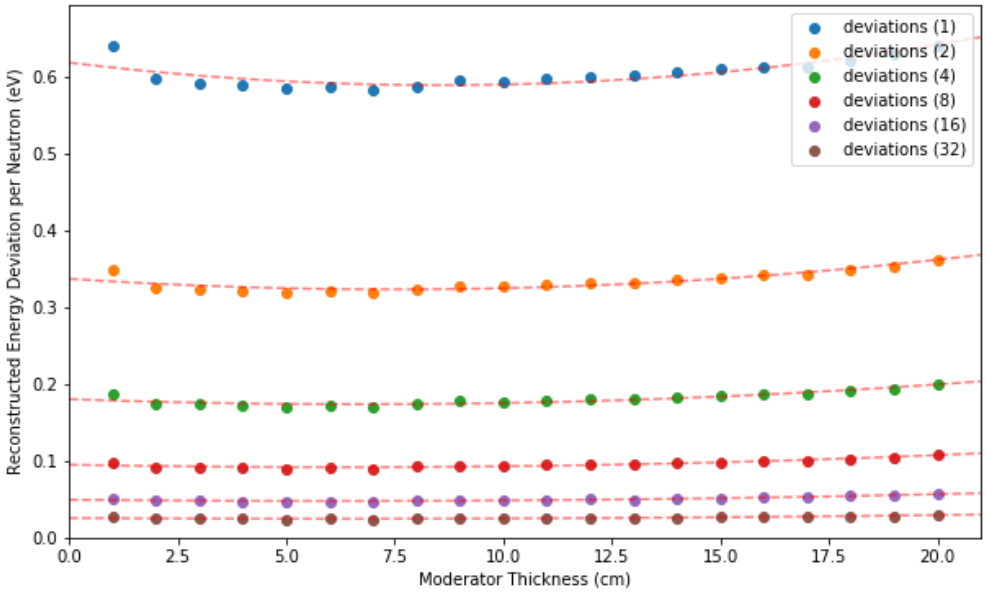

Figure 14: Mean TOF deviation dependence on moderator thickness and flight path distance. Increasing the length of the neutron flight path significantly decreases the TOF reconstruction deviation. The deviation is largely independent of moderator thickness and depends primarily on the length of the neutron flight path.

reconstruction. The geometric specifications of the system are given in Table 7. With this shielding, any neutron that does not enter the collimator is absorbed by the borated absorber-shield. These off-axis neutrons have a negligible effect on the room return background of the system, as can be seen in the discussion in Section 8.2. Many of these off-axis neutrons do, however, reflect from the boron carbide plating surrounding the source into the moderator and are ultimately detected as Line-of-Site (LOS) neutrons in the detector. These internally reflected neutrons actually comprise approximately 25% of detected neutrons, but because the initial scattering event happens on the order of 10 ns, their TOF reconstruction remains highly accurate. The primary source for room-return background are forward-oriented unmoderated neutrons that epithermalize in the rear wall of the room and create an epithermal background. This is further discussed in Section 8.2.

8.1.4 Target

The targets consisted of metallic cylinders 10 cm in diameter and varied between 5 and 10 mm in width. Simulations were performed for five targets consisting of mixes of silver, molybdenum, and tungsten with varied molar ratios. Mixes of silver and tungsten were simulated at 10%, 20%, and 30% silver molar abundance. Mixes of molybdenum and tungsten were simulated at 50% and 75% molybdenum molar abundance. For brevity, isotopic compositions will

Parameter	Measurement
Distance from DT generator to surface of moderator	10 cm
Moderator thickness	9 cm
Distance from surface of moderator to detector	1.845 m
Collimator diameter	20 cm
Outer radius of borated-polyethylene	75 cm
Thickness of boron-carbide plating	10 cm
Thickness of detector shielding	10 cm
Length of detector shielding	40 cm
Cadmium filter thicknesses	5 mm

Table 7: Measurements for portable epithermal DT-source. Neutron flight path can be increased or decreased depending on needs of measurement.

be referenced using their composite elements followed by the atomic percent of the first compound. Using this convention, the mixes are referenced as AgW10, AgW20, AgW30, MoW50, and MoW75, respectively.

Silver, molybdenum, and tungsten were used as proxies for uranium and plutonium for two reasons. First, they are easily available for experimental testing whereas uranium and plutonium are not. Second, silver-tungsten in particular has resonance structures that closely resemble the resonance structures found in mixes of plutonium and uranium. Specifically, the combination of the 5.2 eV resonance in silver and the 4.1 eV resonance found in tungsten creates a sharp feature in the spectra. A system that can adequately resolve these two features from each other should also be able to resolve the low energy features of plutonium and uranium spectra (which have many of these sharp spectral features).

8.2 Results

The system performance was characterized using two criteria: (1) the accuracy of the TOF energy reconstruction and (2) the sensitivity to changes in isotopic composition. Both criteria were characterized using a χ^2 test. The TOF reconstructions were assessed using 140 equally spaced bins between 1 and 15 eV. Above 15 eV, due to the large 18.8 eV resonance in W-186, too few counts were recorded for the χ^2 test to be applicable. For isotopic sensitivity measurements of tungsten-silver samples, the energy range was further restricted to between 1 and 10 eV. The expected attenuation outside this region was nearly identical for all samples due to the lack of further resonances. By necessity, bins containing zero counts were not considered in the calculation of χ^2 statistics.

The goals of this study were to characterize the following:

1. Accuracy of spectral reconstruction was determined by comparing the spectra of the TOF energy reconstruction and the real deposited energy in an idealized detector. Lower χ^2 values indicated better reconstruction with an ideal reconstruction having a χ^2 value of zero.

2. Isotopic sensitivity was determined by directly comparing the TOF energy reconstructions for various isotopic compositions. Higher χ^2 values indicated higher sensitivity.

Both reconstruction accuracy and isotopic sensitivity were highly dependent on the energy range over which the χ^2 value was calculated. Energy reconstruction worsens and sensitivity decreases as the range is expanded to include energies above 30 eV. Neutron production decreases rapidly at energies above 30 eV resulting in a drop in statistics. Inclusion of non-resonant regions in the analysis also substantially reduces the ability to statistically differentiate spectra due to low attenuation probabilities of non-resonant neutrons. Pulse width smearing in the moderator also leads to larger reconstruction errors at higher energies, as discussed in Section 8.1.2.

8.2.1 TOF Energy Reconstruction

In all MC simulations, the distance from the surface of the moderator to the detector was set to 1.845 m as a balance between TOF reconstruction precision and geometrical efficiency. TOF energy calculations used a flight path length of 1.87 meters because it resulted in more accurate reconstructions. Further analysis confirmed that the mean flight path for incident line-of-site epithermal neutrons was approximately 1.87 meters, since final epithermalization occurs for most neutrons between 2 and 3 cm before the rear surface of the moderator.

Figure 15 shows a plot of the energy spectrum of the detected neutrons and the TOF reconstruction for a silver-tungsten mix (at a 10% silver molar abundance). The absorption lines due to the silver resonance (5.2 eV) and tungsten resonances (4.1, 7.7 eV) are clearly apparent in both the deposited and reconstructed energy spectra. The χ^2 statistic for the comparison of the two spectra gives $\chi^2/\text{NDF} = 51/140$. Table 8 shows the χ^2 statistics for various target configurations. The value of χ^2/NDF does not exceed unity for any of the materials or isotopic compositions. A perfect reconstruction should have a chi^2 statistic close to zero.

Further analysis showed that most of the error in the TOF reconstructions is a result of pulse smearing within the moderator. For this purpose, every neutron registered by the detector is back-projected to an extended flight path distance, in the process extrapolating its corresponding TOF using the deposited energy. Then, the energy is again reconstructed from the extrapolated TOF, and the χ^2 comparison is performed for the full sample. This process

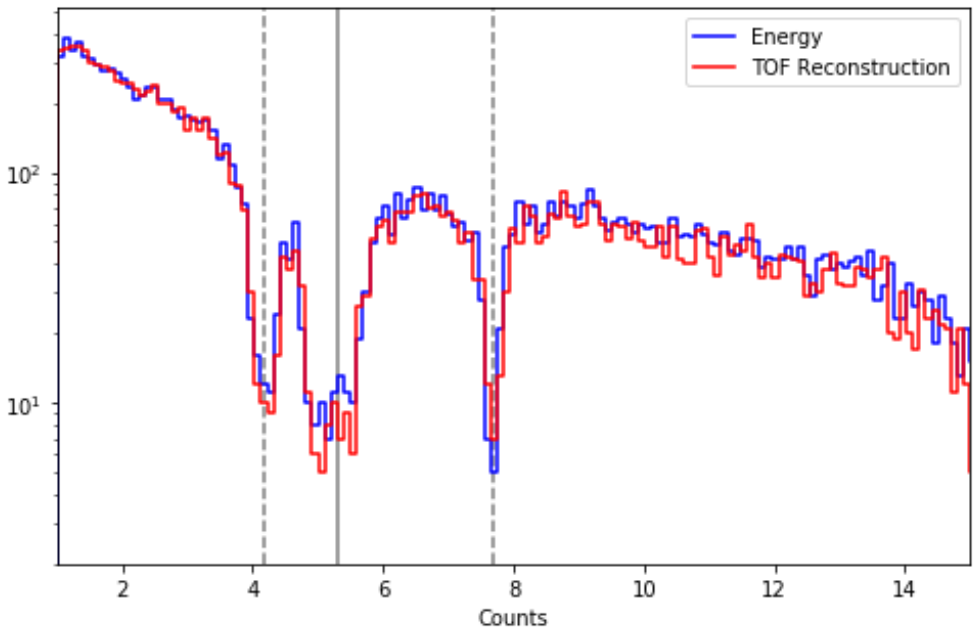

Figure 15: Energy and TOF Reconstruction Comparison. Comparison is for a AgW10 (for explanations of nomenclature see section 8.1.4. The three primary resonances (two for silver, one for tungsten) are apparent and distinct. Dashed lines denote the expected locations for the tungsten and silver resonances.

is repeated for various values of extrapolated distances. Figure 16 shows the relationship between the new χ^2 and the new flight path distance. Each line on the the plot represents a different isotopic configuration. The total neutron fluence is kept constant for all distances in this analysis. We observe a significant decrease in χ^2 value at longer flight paths confirming that the primary source of error in the TOF reconstruction is pulse smearing that occurs during moderation.

For this analysis, the subsample was restricted to neutrons which scattered directly from the moderator into the detector (line-of-sight (LOS) neutrons). LOS neutrons composed $(85.7 \pm 0.2)\%$ of the total neutrons in the original detected sample, with the remaining neutrons having undergone in-scatter inside the collimator or the detector shield. Neutron interactions with boron carbide have about a 5% probability of resulting in a scatter instead of an (n,α) reaction. This background may be further reduced by additional optimizations of the detector shielding or collimator geometry. No detected neutrons were a result of room-return, showing the effectiveness of the optimized configuration.

Target (mm)	[l]Target thicknesses χ^2/NDF	
Ag-W (1:9)	5	51 / 140
Ag-W (1:4)	5	83 / 140
Ag-W (3:7)	5	88 / 140
Mo-W (1:1)	10	66 / 140
Mo-W (3:1)	10	62 / 140

Table 8: χ^2 values for various targets. The reconstructed energy spectra for all targets yield χ^2/NDF less than 1.0, demonstrating reasonably accurate reconstructions. The inaccuracy of the reconstruction is primarily due to pulse smearing within the moderator.

8.2.2 Isotopic Sensitivity

The main value of NRTA is in its ability to identify an object's material composition and to enable isotopic-geometric comparisons between two objects, such as in a warhead verification exercise [48]. We use the system's performance in the latter scenario as the basis for its characterization. The spectral transmission comparisons are performed between objects of different isotopic compositions, enabling characterization of the technique's material discrimination capability.

The isotopic sensitivity of the system was characterized by comparing the TOF reconstructions of varied materials (AgW10, AgW20, AgW30, MoW50, and MoW75). Molar abundances and thicknesses were chosen to optimize transmission probabilities and resonance reconstruction, as well as to allow for practical follow-up experiments. Table 9 shows the χ^2/NDF for the TOF-based spectral comparisons from various isotopic configurations. A comparison of two simulations for the AgW10 (with different random seeds) were used as a control. Materials of various isotopic compositions were compared with each other directly. All simulation results were scaled to $(1.9 \pm 0.3) \times 10^{10}$ total initial events, allowing for direct comparison to each other. To optimize computational efficiency, importance sampling was applied in the neutron angle selection. For a typical DT source the above sample population would correspond to a total measurement time of approximately 30 minutes, assuming an output of approximately 10^9 neutrons/s.

The control comparison (AgW10 vs AgW10) has a reduced χ^2 statistic of approximately order unity which is consistent with two samples drawn from the same distribution. As the molar ratio of the silver is increased in the mix, the χ^2 value compared to AgW10 increases monotonically. Figure 17 shows the spectra for the first four comparisons between mixed compositions of silver-tungsten. The differences between the reconstructions are clearly visible in the spectra. The separation between the 20% and 30% samples deteriorates due to

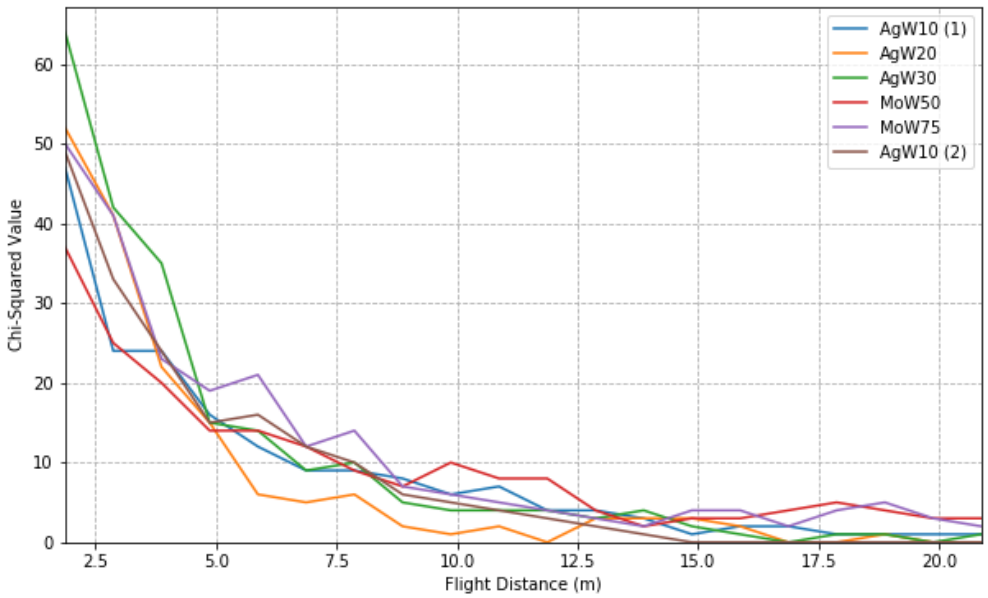

Figure 16: Effect of Flight Path Length on TOF Reconstruction. Most of the error in the reconstruction is introduced by pulse smearing in the moderator. With longer flight paths, this error is minimized, and the chi-squared statistic markedly decreases. The plot shows only the sub-sample of neutrons that scattered directly from the moderator into the detector ($\theta < 0.106$). The impacts on geometric efficiency are ignored in this analysis.

limited statistics within the silver and tungsten resonance structures. This is reflected by the relatively low χ^2 value. The MoW50 and MoW75 separation is also limited, and this is due primarily to low statistics within the resonances combined with a similar overall cross section for both configurations. Additionally, the Mo-98 resonance at 12.1 eV contributes little to the overall separation because it is both relatively weak and degraded by low total neutron flux at those energies. In both cases however, the spectra can be clearly differentiated. With a source that produces 10^9 neutrons/s, the compact configuration can distinguish between different isotopic compositions with less than hour-long measurement times. This could be further reduced as new, more intense sources of neutrons are becoming available.

The applicability of the NRTA approach is specific to both isotopic concentrations and material thicknesses. While the system measures certain spectra highly accurately, other spectra are limited by statistics and overly attenuated resonance structures. These limitations are particularly pronounced for isotopes with large, wide resonances (like tungsten), and will be highly dependent on the thickness of the target and the intensity of the source.

Material	N Ratio 1	N Ratio 2	χ^2/NDF	P-value
Ag-W	10:90	10:90	93 / 90	0.39
Ag-W	10:90	20:80	156 / 90	0.00
Ag-W	10:90	30:70	198 / 90	0.00
Ag-W	20:80	30:70	121 / 90	0.02
Mo-W	50:50	75:25	246 / 160	0.00

Table 9: χ^2 values for spectra separation. Column 1 denotes the mix. Columns 2 and 3 denote the molar ratios being compared. Column 4 denotes the χ^2 test statistic. Separation increases monotonically as the molar abundance of silver in the second mix increases. The control comparison has a χ^2 statistic of approximately order unity. The silver-tungsten and molybdenum-tungsten comparisons are restricted to energy ranges or 1.5-10 eV and 1.5-15 eV, respectively. Outside of these ranges, the attenuation probabilities of different isotopic samples are nearly identical due to the lack of resonances.

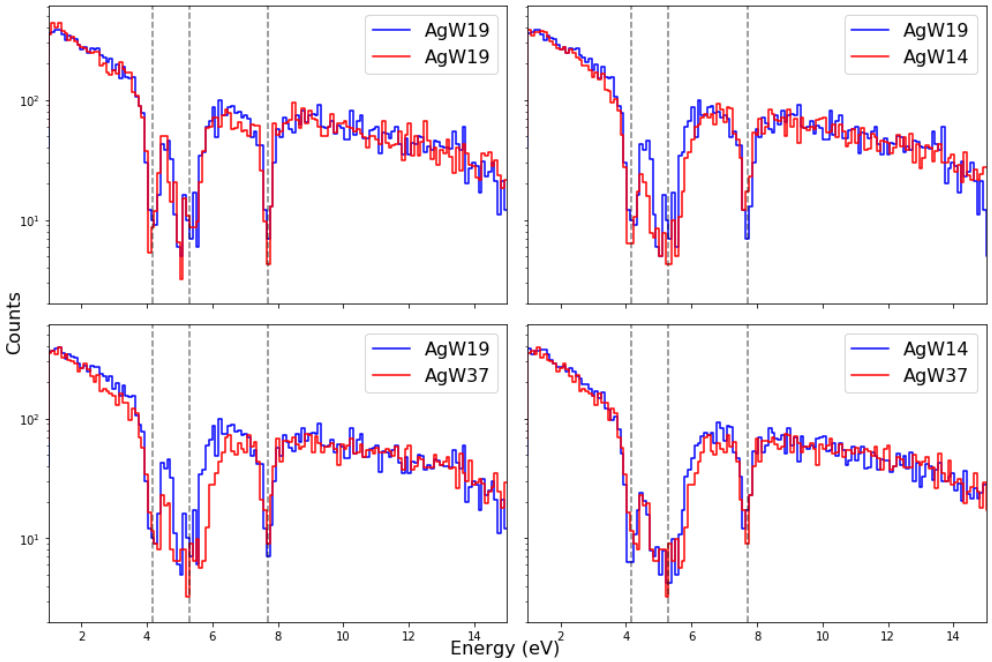

Figure 17: Spectral comparisons for various targets. Visual inspection shows clear differentiation between varied isotopic mixes. Dashed lines represent tungsten and silver resonances.

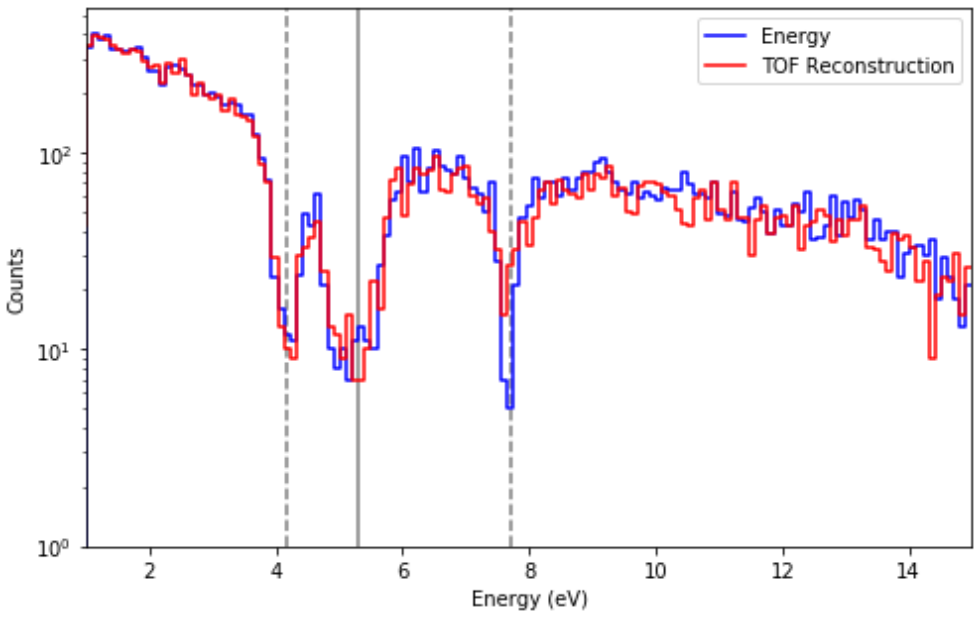

Figure 18: Comparison of AgW10 transmission spectra for an instantaneous neutron generation pulse (blue) and a 5.0 μs pulse width (red) at 5.0 m TOF distance. Note the slight smearing of the narrow resonance at 7.7 eV and the difference in spectra at higher energy. Compare with the spectra in Figures 15 and 17.

8.3 Effects of Neutron Generation Pulse Width

Up to this point, it was assumed that the neutron source generates a neutron beam instantaneously. In reality, the neutron source has a finite pulse width, ranging from several nanoseconds to several microseconds depending on the source. For a compact D-T neutron generator, the pulse was modeled as a square pulse ranging from 0.5 and 5.0 μs in duration with an assumed linear rate of neutron production. This pulse time introduces uncertainty into the t_0 of any given neutron, and as a result, introduces uncertainty in the TOF-reconstructed neutron energy and the reconstructed energy spectra. Therefore there is a trade-off as the pulse time increases: an increase in the neutron beam flux leading to increased statistics, along with a corresponding increase in the uncertainty in neutron energy. This spectral smearing effect is more prominent at higher energies, and, with sufficient statistics, approaches a convolution of the spectrum with the pulse-shape profile. This effect could be mediated by moving the detector further from the source, however, this would reduce the intensity of the neutron flux at the detector.

Table 10 shows the reduced chi^2 values for the various targets. While we observer a slight deterioration of the statistical separation, all spectra can be distinguished from one another. The optimal measuring distance will depend on the isotopic composition and thickness of the

Material	N Ratio 1	N Ratio 2	χ^2/NDF	P-value
Ag-W	10:90	10:90	90 / 90	0.39
Ag-W	10:90	20:80	159 / 90	0.00
Ag-W	10:90	30:70	212 / 90	0.00
Ag-W	20:80	30:70	142 / 90	0.02
Mo-W	50:50	75:25	248 / 160	0.00

Table 10: χ^2 values for spectra separation for a beam smeared with a 5 μs pulse at 5 meters. Column 1 denotes the mix. Columns 2 and 3 denote the molar ratios being compared. Column 4 denotes the χ^2 test statistic. Separation increases monotonically as the molar abundance of silver in the second mix increases. The control comparison has a χ^2 statistic of approximately order unity. The silver-tungsten and molybdenum-tungsten comparisons are restricted to energy ranges or 1.5-10 eV and 1.5-15 eV, respectively. Outside of these ranges, the attenuation probabilities of different isotopic samples are nearly identical due to the lack of resonances.

targets. Due to shorter times of flight for higher energy neutrons, the spectra reconstruction significantly deteriorates at energies above 30 eV. For precise measurements in these higher energy ranges, a flight path needs to be used.

8.4 Polycone Detector Shielding

The design of the compact epithermal neutron source described in the previous sections makes use of simple geometries an materials to facilitate the construction of a functional experimental prototype. Further research will implement these design principles and geometries in the construction of physical epithermal neutron source. However, despite a number of optimizations, some small changes to the current geometry can significantly improve the performance of the system for applications in which precise reconstructions and material identification are paramount. For template-candidate comparisons, the current design is likely sufficiently sensitive to isotopic and geometric composition. For cases that require the identification of completely unknown isotopes, further precision is required.

Simulations results demonstrated that the primary source of background in the current system is in-scattering from the detector shielding and source collimation. These two pathways are described below.

1. Neutrons exit the rear surface of the moderator and scatter off the inner walls of the source collimator. Neutrons have approximately a 20% chance to scatter isotropically in the boron-carbide plating. Some fraction of these neutrons will scatter directly into the detector. In this case, we introduce error into the flight path length since the final scatter occurred somewhere within the detector collimator. This problem actually

decreases as we increase the distance between the source and the detector because the probability that a neutron will scatter into the requisite solid angle decreases and because the length of the source collimator becomes small relative to the total path length which decreases the relative uncertainy in the TOF reconstruction. These type of events represent only a small fraction of the errant neutron background.

2. The more significant source of neutron background is direct in-scattering of line-of-site neutrons from the inner walls of the detector shielding. These neutrons exit the moderator and fly directly into the detector apparatus where they scatter on the boron carbide shielding and enter the detector. in this instance, the probability that neutron scatters directly from the boron carbide shielding into the detector is much higher, since the detector occupies a significantly larger solid angle for the isotropically scattered neutrons. These neutrons down-scatter and fill up the resonance troughs with background signal deteriorating the quality of the TOF reconstruction. This is the dominant form of background in the system.

3. A final source of background is direct scattering from the target itself. Because the primary resonant interaction within the target tends to be elastic scattering, some fraction of scattered neutrons ultimately enter the detector. This effect diminished as the distance between the target and detector is increased.

Simulations showed that between 13% and 15% of detected neutrons were actually background neutrons. On average, only 86% of detected neutrons were direct, line-of-site neutrons from the moderator to the detector–the rest had scattered at some point between moderation and detection. This could be significantly improved by altering the geometry of inner surface of the detector shielding. By implementing a scaled texture on the shielding, the probability of direct in-scatter into the detector can be substantially reduced. Figure 19 shows a comparison between the planar and polycone geometries in the detector shielding.

The polycone shielding utilized in these simulations had an outer radius of 20 cm and was 80 cm in length. The shielding utilized four distinct “teeth" (similar to figure 8.4) that were each 10 cm in width and 6 cm in height. Alternative configurations using sharper teeth and more complex geometries were explored, but did not significantly affect system performance. Geometries which further decrease the background of the system will likely reduce the statistics of the system.

8.4.1 Polycone TOF Reconstruction

Polycone shielding improved performance substantially. Over 95% of detected events were line-of-site neutrons. This further improved as the flight path length was increased and the

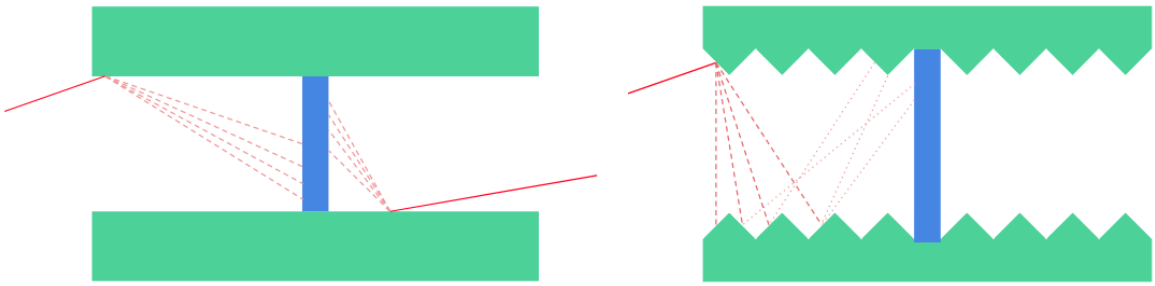

Figure 19: Comparison of polycone and plane detector shielding. The polycone configuration substantially reduces the probability of a direct in-scatter by forcing most incident neutrons to scatter multiple times within the boron-carbide before hitting the detector. Such a design can theoretically be further optimized through adaptive shaping of the “teeth"; however these further changes to the scaling geometry did not substantially improve the performance of the system. Remaining background is primarily a result of source-collimator scattering and target scattering as described in Section 8.4.

effects of collimator and target scattering diminished. These improvements were reflected in significantly more accurate TOF reconstructions. Figure 20 shows the TOF reconstruction for 5 mm of AgW10 mix. As earlier, the dashed lines denote the silver resonances, while the solid line denotes the tungsten resonance. Resonances are completely “blacked out" indicating a minimization of most background and accurate TOF reconstructions. The reduced χ^2/NDF is 73/132 indicating an accurate reconstruction.

With the polycone shielding virtually all the remaining error in the final reconstruction is a result of moderator time smearing. This becomes apparent in a number of spectra at the 7.7 eV silver resonance. As in the case of the cylinder shield, most of the inaccuracy in the reconstruction is a result of moderator time-smearing. As we move to longer flight paths, this χ^2/NDF begins to approach zero. Figure 21 shows the relationship between path length and chi-squared value for a polycone configuration. Reconstruction is comparable to the plane cylinder design at all path lengths.

The polycone shielding configuration offers obvious advantages over the simple cylinder configuration at the cost of a more complicated design. Further improvements could likely be made by implementing a polycone geometry with the source collimator. For practical reasons, these types of modifications were not considered in this analysis. The polycone optimized system is capable of highly accurate (nearly flawless) TOF reconstructions for various energy spectra and may have applications for materials characterization in a variety of fields.[34] [54]

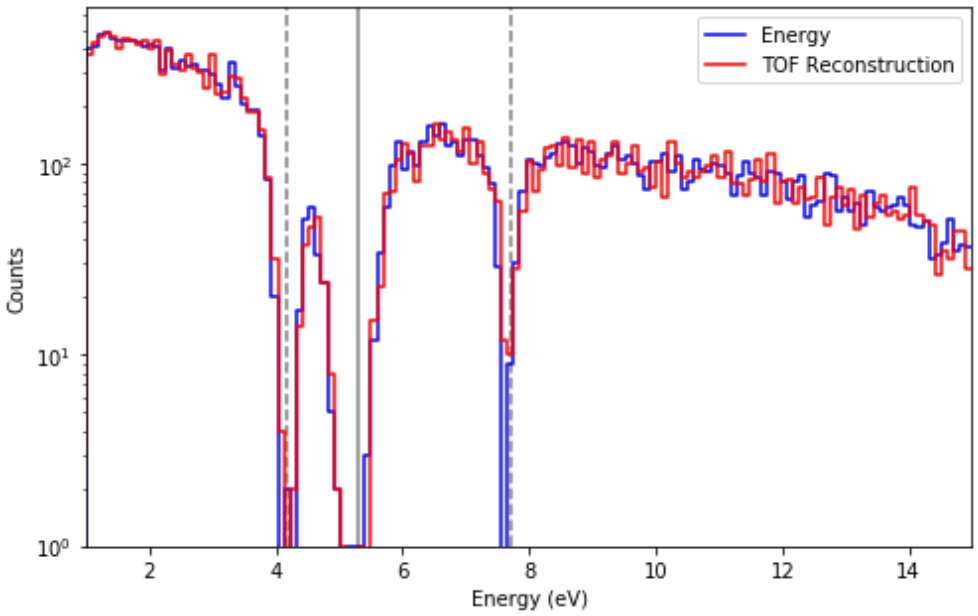

Figure 20: TOF reconstruction of silver-tungsten target using polycone detector shielding. The addition of the polycone shielding significantly improves the reconstruction of the resonances. The mitigation of down-scatter eliminates all counts in the 4.1 eV and 5.2 eV resonances. The filling of the 7.7 eV resonance does not represent real background. Rather, with a short path length of only 1.87 m, moderator time-smearing causes error in the TOF reconstruction at this higher energy resonance. The effect decreases with longer path lengths.

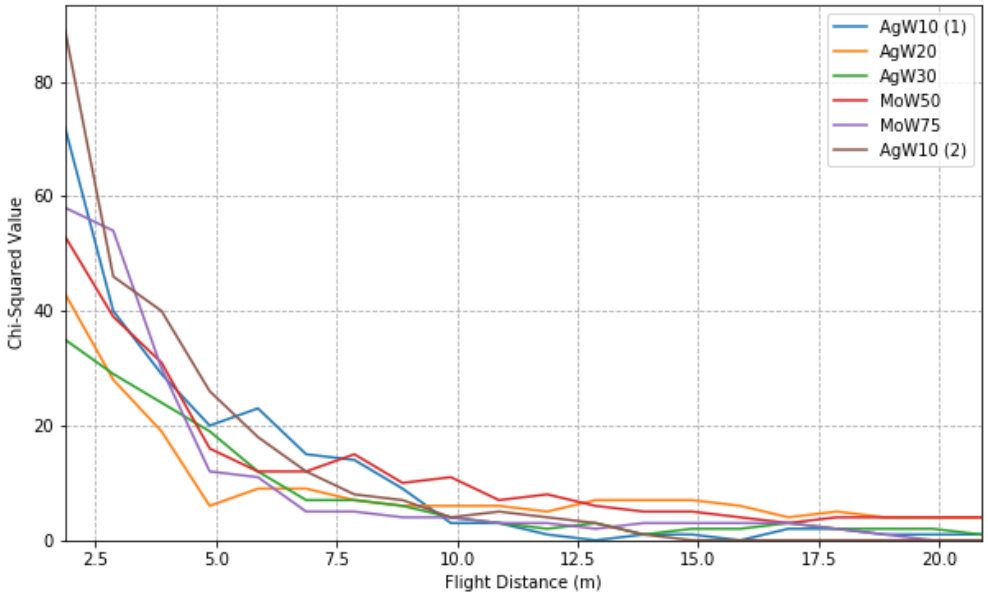

Figure 21: Relationship between path length and chi-squared value for TOF reconstruction. As in Figure 14, increases in the path length significantly improve the chi-squared value for the TOF. However, with the implementation of the polycone shielding, the χ^2 values are comparable to those for the cylinder shielding and drop to virtually zero beyond 10 meters (indicating nearly perfect TOF reconstruction).

8.4.2 Polycone Spectra Differentiation

Utilizing the polycone geometry also continues to provide highly accurate spectra differentiation across all isotopic configurations. Visually, the reconstructed spectra better represent the attenuation probabilities for the given targets. These resonances are significantly better resolved using the polycone design. They completely “black out", and the full resonance shape is observable in the data. Figure 22 shows the comparisons between various targets for the polycone design. In all cases the resonances are apparent and the spectra are visually distinct from one another. Compare the spectral reconstruction with those in figure 17 to see the significant improvement.

In these comparisons, the effect of moderator pulse smearing can be observed. Because these measurements were taken at 1.87 meters in order to maximize the computational efficiency of the simulation, the 1 μs (approximate) smearing in the epithermalization time ultimately limits the TOF reconstruction. The 4.1 eV and 5.2 eV resonances are perfectly reconstructed, but because the 7.7 eV resonance is so narrow and is more affected by smearing in time space, the system fails to reconstruct a “blacked out" resonance. Simulations at longer flight paths largely mitigate this.

Table 11 shows the χ^2/NDF values for comparisons between different targets. In all cases

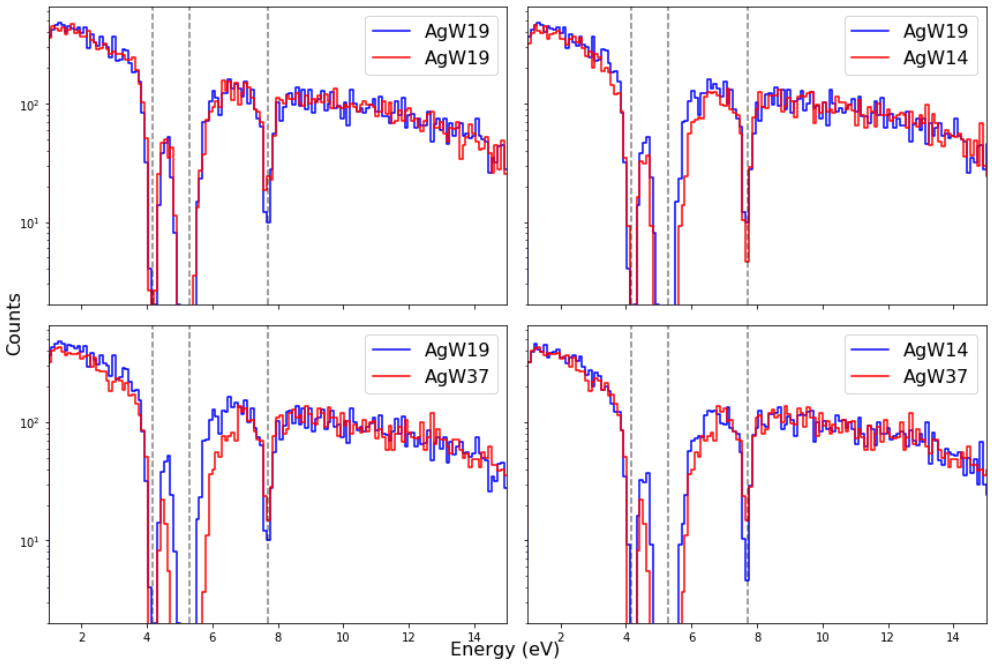

Figure 22: The polycone shielding yields significantly improved spectra reconstruction for all targets with better resolved resonance structures. By removing most of the background and down-scattered neutrons, the full shape of the resonance is observable and differentiation improves over the cylindrical shielding designs.

but the molybdenum, the separation has improved over the previous cylindrical design. Silver and tungsten have similarly shaped non-resonant neutron cross sections, so the only places in which the mixes are differentiated are within the resonances. Specifically the cross sections between 1 and 15 eV for Ag-109 and W-186 have very similar shapes. Molybdenum, however, has a much lower non-resonant cross section than tungsten or silver in the 1 eV to 15 eV region, apparent in figure 23. When the chi-squared values for these spectra are calculated, a significant fraction of the overall separation stems from non-resonant differentiation between tungsten and molybdenum abundances. The primary effect of the polycone configuration is to better resolve the resonances by reducing background. Non-resonant differentiation remains equally strong in both configurations, so the polycone does not significantly improve the statistical differentiation of the molybdenum-tungsten mixes.

Despite this, because the shape of the resonances is better resolved for the polycone, the user receives more information about the isotopic composition of the material. Non-resonant can improve the confidence of direct comparisons between different targets, but is not particularly useful for inferring the composition of those targets, since many isotopes share similar non-resonant structure (such as silver and tungsten). Inference can be further improved by expanding the energy range of interest. As more resonant structures are introduced into

Material	N Ratio 1	N Ratio 2	χ^2/NDF	P-value
Ag-W	10:90	10:90	102 / 85	0.10
Ag-W	10:90	20:80	189 / 83	0.00
Ag-W	10:90	30:70	324 / 81	0.00
Ag-W	20:80	30:70	128 / 81	0.00
Mo-W	50:50	75:25	216 / 151	0.00

Table 11: χ^2 values for spectra separation in a polycone configuration. Column 1 denotes the mix. Columns 2 and 3 denote the molar ratios being compared. Column 4 denotes the χ^2 test statistic. The silver-tungsten and molybdenum-tungsten comparisons are restricted to energy ranges or 1.5-10 eV and 1.5-15 eV, respectively. As in previous examples the separation improves monotonically with increasingly differentiated material mixes.

Material	N Ratio 1	N Ratio 2	χ^2/NDF	P-value
Ag-W	10:90	10:90	86 / 86	0.48
Ag-W	10:90	20:80	163 / 85	0.00
Ag-W	10:90	30:70	288 / 84	0.00
Ag-W	20:80	30:70	101 / 82	0.08
Mo-W	50:50	75:25	240 / 158	0.00

Table 12: χ^2 values for spectra separation in a polycone configuration with 5 μs pulse smearing at 5 m. See Table 11 caption for further explanation. The χ^2 values generally decrease in the presence of the pulse smearing (except in the case of molybdenum mixes due to the effects discussed in section 8.4.2). Additionally, the AgW20 and AgW30 comparison is no longer statistically significant. However, the two spectra remain visually distinct and would likely become differentiated with additional statistics.

the data (at higher energies) fewer possibly combinations of isotopes can feasibly result in an observed spectra.

8.4.3 Polycone Pulse Width Smearing

When a 5 μs pulse width is applied to the data, the reconstructions deteriorate although it remains possible to differentiate most of the targets. Table 12 shows the reduced χ^2 values for the various target comparisons with the implementation of a 5 μs pulse at a 5 meter path length. The χ^2 values generally decrease as expected. The molybdenum mixes actually retain a larger χ^2 largely due to the non-resonant attenuation affect that were discussed in section 8.4.2. The comparison between AgW20 and AgW30 is no longer significant with the implementation of the pulse smearing; however, visual observation of the two spectra shows a clear differentiation, so it is likely that the comparison would become statistically significant at longer measurement times.

The affects of pulse width smearing on the polycone configuration are more apparent than the effects on the cylindrical design. This is because the the pulse smearing primarily functions to smooth and distort sharp features in the spectra such as the resonance structures. Because the resonances are better resolved with the polycone configuration, the effect of this smearing is exacerbated when compared to the cylindrical case. In both cases, extending the beam path would significantly improve the reconstruction at the cost of statistics.

8.4.4 Analytical Spectra Reconstruction

Section 8.4.2 shows that the system can confidently distinguish between various targets. This sensitivity has clear applications for template-like warhead verification regimes. In such a regime, an inspector would obtain a golden copy of a host's warhead, and then compare the fingerprints of the golden copy and those obtained from candidate warheads. The proposed system would be highly sensitive to most hoaxing attempts using direct comparison between the golden copy and candidate.

However, an epithermal TOF system has potential applications for materials science, stockpile stewardship, and archaeology as well. These fields would require the system to be capable of inferring the isotopics of an unknown material. This would require reconstructions that closely resemble the predicted attenuation spectrum for a given set of isotopes and thicknesses. Ideally, such a system would reproduce the spectra expected from the known cross sections for a full range of possible isotopes. Figure 23 shows the known cross section data for silver, molybdenum, and tungsten. These cross sections can be used in conjunction with basic attenuation calculations to produce expected attenuation spectra for various target configurations.

To test whether the system is accurately reproducing the analytical expectations for the targets, the MC reconstructed spectra were compared with analytically derived data. The cross sections for silver, molybdenum, and tungsten were used to build attenuation spectra for the different targets used in the MC simulations. These attenuation spectra predicted the attenuation probability for a neutron at a given energy between 1 eV and 20 eV. These attenuation spectra were then combined with open beam data to create “analytical spectra", in which the spectra features were isolated *only* to the physical processes described by the cross section data.

These “analytical spectra" were then normalized to the intial events of the various MC TOF spectra and compared directly with the reconstruction for each of the targets. In all cases, the energy range was restricted to 1 eV through 10 eV, as this is where the primary resonant features of all spectra are. Expanding the energy would artificially improve the accuracy of the reconstruction by including non-resonant regions in the calculation. Figure 24

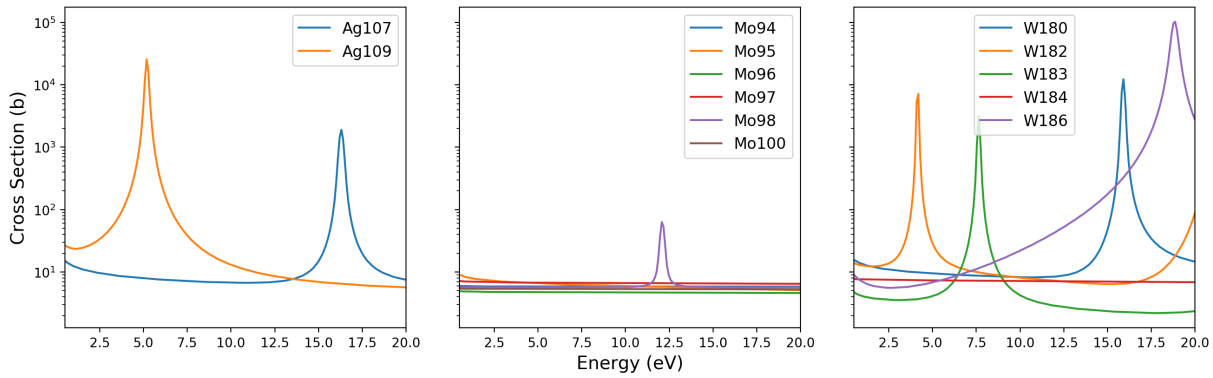

Figure 23: Cross sections for isotopes of silver, molybdenum and tungsten (from left to right). Molybdenum has a lower non-resonant cross section than silver or tungsten which leads to non-resonant differentiation between different mixes of molybdenum. These non-resonant effects are not reliable when trying to infer isotopics from a given measurement. The known cross sections can be used to calculate predicted attenuation curves to compare directly with reconstructed spectra. Data from Brookhaven National Lab.

shows the comparison of the analytic and MC spectra of AgW10. In all cases the analytical spectra were compared to the true energy spectra from the MC simulation. This was done to avoid the effect of TOF smearing in the moderator for the sake of direct comparison. At longer flight paths, the TOF reconstruction has been shown to approach the true energy spectrum.

It is visually apparent that the two spectra are extremely similar. This consistency was true for all five of the targets. In all cases, the analytic and MC spectra were not visually distinguishable. For each of the target configurations, the χ^2/NDF was calculated to determine whether the spectra were statistically similar. Table 13 shows the results of the χ^2 tests. In all cases, the analytical spectrum was not statistically different from the MC spectrum.

Target	Thickness (mm)	χ^2/NDF	P-value
Ag-W (10:90)	5	83 / 81	0.41
Ag-W (20:80)	5	68 / 78	0.78
Ag-W (30:70)	5	90 / 79	0.20
Mo-W (50:50)	10	80 / 85	0.63
Mo-W (75:25)	10	77 / 88	0.79

Table 13: χ^2 values for various targets compared with an analytical construction of the data using known cross sections. Analytical constructions are generally consistent with results from the MC simulations.

These results demonstrate two primary characteristics of the system. First, because the

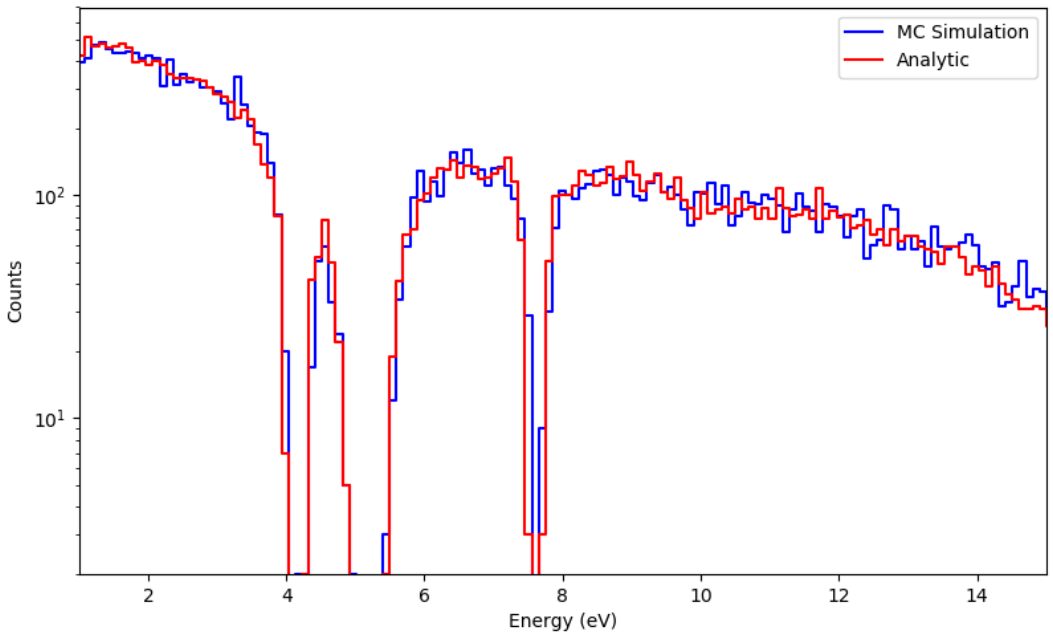

Figure 24: A comparison of an analytically constructed spectrum using cross section data and an open beam measurement with results from the MC simulation for AgW10. The comparison shows a tight correspondence between the two spectra. This shows (1) that the primary features of the reconstructed spectra are the result of isotopic scattering and (n,γ) reactions in the target and (2) that the system has inference power for characterizing the isotopic compositions of unknown material.

analytical spectra are so well reproduced, we can be confident that the primary features and resonant structures observed in the MC simulations are results of isotopic scattering and (n,γ) in the target. We have effectively isolated the targets spectrum from most of the potential background. Second, the system is highly capable of inferring the isotopics of unknown materials. This inference would require the design of a predictive algorithm and would likely require more statistics than are currently being used for direct spectra comparison. However, it remains likely that the system is capable of these types of applications.

8.5 Summary of DT-Source Designs

The proposed system is capable of highly accurate TOF reconstructions and is highly sensitive to changes in isotopic composition of the target. Current errors in TOF reconstruction are small and due primarily to pulse smearing within the moderator and in-scattering from the detector shielding. These can be further mitigated by increasing the neutron flight path length, and modifying the inner surface of the detector shielding. The sensitivity to isotopic composition makes the system an ideal candidate for on-site measurements of sensitive nuclear material. With further work the system may be able to characterize and identify unknown samples of material with epithermal resonance structures.

Additionally, the system has been shown able to reliably reconstruct spectra that are similar to the results predicted by analytical use of the cross sections. This expands the scope of the systems uses to include applications that require isotopic inference and material characterization. Ideally, the system would be deployed with a set of algorithms that utilize either parameterization and gradient descent or machine learning in order to estimate the isotopic compositions of unknown samples.

The use of compact neutrons sources has the potential to significantly expand the utility and applicability of NRTA in a variety of fields. The preliminary Monte Carlo results in this work indicate the feasibility of a DT-based NRTA system. Though current analysis has focused on the optimization of DT-based sources alone,, deuterium-deuterium sources, and LinAc-based photodisintegration sources may also provide viable methods for compact neutron generation. Future research should explore these alternatives.

NRTA is powerful method for isotopically sensitive radiography, and the techniques and optimization described in this analysis and planned extensions demonstrate strong potential for arms-control, material science, and archaeology. The capability of on-site isotopic imaging will provide researchers and policy-makers with a novel tool for meeting objectives in materials analysis and nuclear diplomacy.

9 Conclusions

Compact neutron and physical cryptography may enable on-site measurements of special nuclear material with high levels of information security. Current research has demonstrated that appropriately optimized compact sources could feasibly be implemented for TOF applications in both weapons verification and a variety of other fields. While not as accurate as dedicated facilities, these designs may enable a flexible isotopic characterization of unknown material in which use of a permanent facility is either unavailable or impractical.

Advances in physical cryptography, particularly the development of tomographic systems solve many of the technological barriers to warhead verification. These systems have relatively high tolerances for alignment, measurement times, and experimental set up. The materials and objects involved are either readily available or easily constructed. Combining this approach with compact neutron sources may enable on-site weapons verification as a some part of a future treaty regime.

To improve confidence in the system, the Laboratory for Nuclear Security currently plans to construct an experimental prototype for compact TOF measurement. While early designs will likely incorporate a DT source, future designs will likely move toward portable linear accelerators and photo-disintegration on beryllium targets due to higher fluxes and shorter pulse times. Alternatively, next generation neutron sources currently in development may prove to be viable options for use in these compact sources with neutron fluxes five orders of magnitude greater than current models. Advances in the portability and intensity of LINACs and DT sources make these designs and implementations increasingly feasible.

These designs support an important niche in treaty enforcement and weapons verification. The problem of information security has long been an obstacle for direct warhead verification, and a as a result, previous treaty regimes have focused exclusively on the disassembly of delivery vehicles as proxies for strike capability. If the world wants to truly reduce the number of existing nuclear warheads, direct verification will be essential. This research addresses many of the problems that have plagued discussions of these regimes in the past.

Continued work on spectrum post-processing and the construction may pave the way for future treaty negotiations and may ultimately provide policy-makers with the tools they need to move the world towards a disarmed future.

Early work also demonstrates promise for LinAcs as potential neutron sources for these compact systems. Using 3 MeV LinAcs in conjunction with bremsstrahlung and photodisintegration on deuterium would produce a narrow band of relatively low energy neutrons requiring significantly less shielding than the designs discussed in this work. Current simulations have demonstrated the feasibility of this approach for NRTA, but further work is required to fully

optimize these LinAc systems.

Significant research has focused on the use of LinAcs as neutron sources for NRTA although most work has not emphasized compactness or portability. LinAc neutron sources can be designed with significantly lower initial neutron energy and can be operated with shorter pulses than DT generators. Historically LinAcs have been used to accurately characterize reactor fuel samples and other nuclear data [55]. Many of these sources have been optimized for use in the thermal region, but their distinct advantages apply in the epithermal range as well [56]. Current work will focus on using design innovations from LinAc sources to optimize a compact source for verification applications.

Even in 2019, nuclear weapons continue to pose a grave threat to the stability and security of global politics. Though efforts to curb proliferation have been largely successful, far too many weapon systems remain deployed or stockpiled. The only conceivable path towards future disarmament efforts is the design of new technical means for verification and nuclear measurement. Hopefully, these techniques will empower a new generation of politicians to continue moving the world closer to one in which massive nuclear stockpiles only exist in memory.

10 Acknowledgements

My fascination with science and engineering has been a lifelong journey facilitated by a number of important people in my life. Parents, grandparents, family-members, teachers, mentors, and advisors have, at every step of the way, encouraged and nurtured my interest in discovery and learning. Their efforts and their support have provided me with the values and enthusiasm I've carried with me into most (not all) my academic endeavors. My time at MIT, and the work that I've done here potentially represents the last purely academic experience I'll have, and I'd like to offer a special thank you to my thesis advisor, Dr. Areg Danagoulian, for coloring this experience with interesting questions, motivating research, and sound guidance.

References

[1] Jie Yan and Alexander Glaser. Nuclear warhead verification: A review of attribute and template systems. *Science Global Security*, 23(3):157–170, 2015.

[2] H. M. Kristensen and Robert S. Norris. Status of world nuclear forces. *Federation of American Scientists*, Nov 2018.

[3] Alexander Glaser and Robert J. Goldston. A zero knowledge protocol for nuclear warhead verification. 2014.

[4] Scott Kemp and Areg Danagoulian. Physical cryptography of nuclear warheads. *Proceedings of the National Academy of Sciences*, 113(31):8618–8623, 2016.

[5] C. Glaser. The flawed case for nuclear disarmament. *Survival*, 40(1):112–128, 1998.

[6] Lawrence S. Wittner. *Confronting the bomb: a short history of the world nuclear disarmament movement*. Stanford University Press, 2009.

[7] *Narrative Summaries of Accidents Involving U.S. Nuclear Weapons 1950- 1980*. GPO, 1981.

[8] Charles Perrow. Normal accidents: Living with high risk technologies. *Princeton University Press*, 1984.

[9] J. Reason. Human error: models and management. *Bmj*, 320(7237):768–770, 2000.

[10] Robert B. Glassman. Persistence and loose coupling in living systems. *Behavioral Science*, 18(2):83–98, 1973.

[11] Ira Glass and J. Richman. Human error in volatile situations, Dec 2017.

[12] Denise M. Rousseau and Scott D. Sagan. The limits of safety: Organizations, accidents, and nuclear weapons. *Administrative Science Quarterly*, 41(1):200, 1996.

[13] Eric Schlosser. *Command and control:*. Penguin Books, 2014.

[14] G. Perkovich. *Nuclear Power and Nuclear Weapons in India, Pakistan, and Iran*, page 189–199. Brassey's, 2002.

[15] Richard Rhodes. *The making of the atomic bomb*. Simon Schuster Paperbacks, 2012.

[16] Motoko Rich. Survivors recount horrors of hiroshima and nagasaki, May 2016.

[17] L. Rothman. After the bomb: Survivors of hiroshima and nagasaki share their stories.

[18] Senate. *The New START Treaty (Treaty doc. 111-5): hearings before the Committee on Foreign Relations, United States Senate, One Hundred Eleventh Congress, second session, April 29, May 18, 19, 25, June 10, 15, 16, 24, and July 15, 2010*. U.S. G.P.O., 2010.

[19] Wyn Q. Bowen, Hassan Elbahtimy, Christopher Hobbs, and Matthew Moran. Verification in the nuclear arena: Nature, significance and practice. *Trust in Nuclear Disarmament Verification*, page 19–49, 2018.

[20] F. Waller and J. Larsen. *Strategic Nuclear Arms Control*. Lynne Rienner, 2002.

[21] S. Lodgaard. *The Process of Nuclear Disarmament*. Victoria House, 2000.

[22] S. Fetter and J. Rotblat. *Verifying Nuclear Disarmament*, page 71–101. Westview Press, 1998.

[23] Stephen M. Walt. Alliance formation and the balance of world power. *International Security*, 9(4):3, 1985.

[24] Drew Fudenberg and Jean Triole. *Game Theory (The MIT Press)*. MIT Press, 1991.

[25] Thucydides and R. W. Livingstone. *The history of the Pelopennesian War*. Galaxy Books, 1960.

[26] Thomas Hobbes and Nancy A. Stanlick. *The essential Leviathan: a modernized edition*. Hackett Publishing Company, Inc., 2016.

[27] Carl von Clausewitz. *Clausewitz On War*. Penguin Books Inc.

[28] John Nash. Non-cooperative games. *The Annals of Mathematics*, 54(2):286, 1951.

[29] Charles W. Kegley. *Controversies in international relations theory: realism and the neoliberal challenge*. Peking University Press, 2004.

[30] Mark Bassin. Race contra space: the conflict between german geopolitik and national socialism. *Political Geography Quarterly*, 6(2):115–134, 1987.

[31] Sam G. Mcfarland, Vladimir S. Ageyev, and Marina A. Abalakina-Paap. Authoritarianism in the former soviet union. *Journal of Personality and Social Psychology*, 63(6):1004–1010, 1992.

[32] Michael N. Barnett. *Dialogues in Arab politics: negotiations in regional order*. Columbia University Press, 1998.

[33] Jozef Goldblat. *Arms control: the new guide to negotiations and agreements*. PRIO, 2002.

[34] Kenneth W Abbot. Trust but verify: The production of information in arms control treaties and other international agreements. *Cornell International Law Journal*, 26(1), 1993.

[35] Duncan MacArthur. *Use of information barriers to protect classified information.* Los Alamos National Laboratory (LANL), 1998.

[36] V. Hamilton and B. Wood. *An Information Security Approach to Information Barriers for Radiation-Based Verification of Classified Materials.* Sandia National Laboratories, 1999.

[37] S. Fetter, T. Cochran, F. v. Hippel, and R. Sagdeev. *Measurement of Gamma Rays from a Soviet Cruise Missile*, page 379–399. Gordon and Breach Science Publishers, 1990.

[38] S. Fetter and V. Frolov. *Detecting Nuclear Warheads*, page 265–369. Breach Science Publishers, 1990.

[39] R. Sagdeev and R. Sagdeev. *Passive Detection of Nuclear-Armed SLCMs*, page 369–379. Gordon and Breach Science Publishers, 1990.

[40] Cesar Sastre and P. Vanier. *CIVET a Controlled Intrusiveness Verification Technology.* Brookhaven National Lab (BNL), 1988.

[41] P. Zuhoski, J. P. Indusi, and P. E. Varrier. Building a dedicated information barrier system for warhead verification and sensitive item verification. *42nd Annual INMM Meeting*, Jul 2001.

[42] Dean Mitchell and Keith M. Tolk. *Trusted Radiation attribute detection system (TRADS).* Sandia National Laboratories, 2000.

[43] L G Chiang. Nuclear materials identification system operational manual. *ORNL Oak Ridge National Lab (US)*, 2001.

[44] Richard B Williams. *Advances in Information Barrier Design.* Los Alamos National Laboratory (LANL), 2005.

[45] James Fuller. *The functional requirements and design basis for information barriers.* Pacific Northwest National Lab (PNNL), 2012.

[46] S Goldwasser, S Micali, and C Rackoff. The knowledge complexity of interactive proof-systems. *Proceedings of the seventeenth annual ACM symposium on Theory of computing - STOC 85*, 1985.

[47] Sebastien Philippe. Zero-knowledge differential isotopic comparison of special nuclear materials. *Proceedings of the 57th Institute of Nuclear Materials Management Annual Meeting*.

[48] Jake J. Hecla and Areg Danagoulian. Nuclear disarmament verification via resonant phenomena. *Nature Communications*, 9(1), 2018.

[49] J. Li, R. Dahal, S. Majety, J.y. Lin, and H.x. Jiang. Hexagonal boron nitride epitaxial layers as neutron detector materials. *Nuclear Instruments and Methods in Physics Research Section A: Accelerators, Spectrometers, Detectors and Associated Equipment*, 654(1):417–420, 2011.

[50] Marco F Duarte. Single-pixel imaging via compressive sampling. *IEEE singal processing magazine*, 15(2):83–91, 2008.

[51] Adrian S. Losko, Sven C. Vogel, H. Matthias Reiche, and Heinz Nakotte. A six-axis robotic sample changer for high-throughput neutron powder diffraction and texture measurements. *Journal of Applied Crystallography*, 47(6):2109–2112, 2014.

[52] S. Agostinelli et al. GEANT4: A simulation toolkit. *Nucl. Instrum. Meth.*, A506:250–303, 2003.

[53] P325 Neutron Generator, a compact neutron generator for maximum versatility. `http://www.thermo.com.cn/Resources/200802/productPDF_24486.pdf`, 2019. Last accessed on 02.12.2019.

[54] George Kour and Raid Saabne. Real-time segmentation of on-line handwritten arabic script. In *Frontiers in Handwriting Recognition (ICFHR), 2014 14th International Conference on*, pages 417–422. IEEE, 2014.

[55] James W Behrens, Ronald G Johnson, and Roald A Schrack. Neutron resonance transmission analysis of reactor fuel samples. *Nuclear technology*, 67(1):162–168, 1984.

[56] CD Bowman. Efficient neutron production using low-energy electron beams. *Nuclear Science and Engineering*, 75(1):12–15, 1980.